J. Fluid Mech. (2011), *vol.* 678, *pp.* 348–378. © Cambridge University Press 2011
doi:10.1017/jfm.2011.116

Acoustic implications of a thin viscous boundary layer over a compliant surface or permeable liner

E. J. BRAMBLEY†

Department of Applied Mathematics and Theoretical Physics, University of Cambridge, Centre for Mathematical Sciences, Wilberforce Road, Cambridge CB3 0WA, UK

(Received 1 September 2009; revised 14 November 2010; accepted 6 March 2011; first published online 26 April 2011)

This paper considers the implications of a high-Reynolds-number thin parallel boundary layer on fluid–solid interaction. Two types of boundaries are considered: a *compliant* boundary which is flexible but impermeable, such as an elastic sheet or elastic solid, and a *permeable* boundary which is rigidly fixed, such as a perforated rigid sheet. The fluid flow consists of a steady flow along the boundary and a small time-dependent perturbation, with the boundary reacting to the perturbation. The fluid displacement due to the perturbation is assumed to be much smaller than the boundary-layer thickness. The analysis is equally valid for compressible and incompressible fluids. Numerical examples are given for compressible flow along a cylindrical duct, for both permeable and compliant cylinder walls. The difference between compliant and permeable walls is shown to be dramatic in some cases. High- and low-frequency asymptotics are derived, and shown to compare well to the numerics. When used with a mass–spring–damper boundary, this model is shown to lead to similar, but not identical, temporal instability with unbounded growth rate to that seen for slipping flow using the Myers boundary condition. It is therefore suggested that a regularization of the Myers boundary condition removing the unbounded growth rate may lead to, or at least inform, a regularization of the model presented here.

Key words: aeroacoustics, compressible flows, wave–structure interactions

1. Introduction

The modelling of small perturbations to a steady fluid flow past a deformable object has been widely studied due to its many applications, including sound damping in automotive and aeroengine acoustic silencers, and physical stability considerations such as panel flutter. One simple and oft-used model is to approximate the steady fluid flow as being uniform (for example, Koch & Möhring 1983; Brazier-Smith & Scott 1984; Crighton & Oswell 1991; Peake 1997; Abrahams & Wickham 2001; Lucey, Sen & Carpenter 2003). The boundary condition applied at the fluid–solid interface in this case is to match the fluid and solid displacements. This was justified, apparently independently, by Eversman & Beckemeyer (1972) and Tester (1973) by considering the limit of a vanishingly thin inviscid boundary layer at the fluid–solid interface. This helped clear up some considerable confusion that previously existed between matching velocity or displacement (Rice 1969, for example), and this

† Email address for correspondence: E.J.Brambley@damtp.cam.ac.uk

https://doi.org/10.1017/jfm.2011.116 Published online by Cambridge University Press

boundary condition is now almost universally applied under the name of the Myers boundary condition (so named because of the work of Myers 1980).

There has been considerable debate over the mathematical and numerical stability of the Myers boundary condition when applied to acoustics over deformable surfaces with slipping flow (for example, Tam & Auriault 1996; Rienstra 2003, 2007; Richter & Thiele 2007). In the author's opinion there is a deficiency in this mathematical model which prevents a correct mathematical stability analysis (Brambley 2009). The mathematical question of stability of the boundary condition is removed for non-slipping flows. In light of this, and in search of greater accuracy for numerical and analytic solution when compared with experiments, there has been growing interest in recent years in modelling a finite-thickness shear layer such that the flow at the boundary is non-slipping (for example, Aurégan, Starobinski & Pagneux 2001; Vilenski & Rienstra 2007).

Sound within sheared flow, both within and outside boundary layers, is often studied using the inviscid equation attributed to Pridmore-Brown (1958) or its cylindrical counterpart (e.g. Mungur & Plumblee 1969), which neglects temperature variation and viscous and thermal dissipation (Eversman 1971; Mariano 1971; Goldstein & Rice 1973; Jones 1977; Nagel & Brand 1982; Campos & Serrão 1998; Vilenski & Rienstra 2007). These dissipative terms were included by Nayfeh (1973) when considering viscous flow over a permeable boundary, although gradients of the mean flow at the wall were assumed to be $O(1)$, and so this analysis is not applicable to thin boundary layers. More recently, Aurégan *et al.* (2001) included dissipative terms in their analysis while allowing the boundary layer to be thin. They found that the Myers boundary condition was attained only for high frequencies, while for low frequencies they predicted normal mass flux to be constant across the boundary layer (leading to matching normal velocity in the absence of density gradients). These conclusions were derived under the assumption that the velocity and temperature difference across the boundary layer are small. Even more recently, Renou & Aurégan (2010) showed that incorporating viscosity within the boundary layer is necessary in order to accurately correlate mathematical and numerical results with experiments.

The purpose of this paper is to investigate the same situation considered by Aurégan *et al.* (2001), but without the restriction of small changes in velocity and temperature across the boundary layer, and allowing for both compliant and permeable boundaries. The assumptions made here are that the Reynolds number is large, that the time-dependent perturbations are small and that the boundary-layer flow is parallel (meaning that all mean-flow variables within the boundary layer are functions of only the distance from the boundary). These assumptions are also made in numerous other works (for example, Eversman & Beckemeyer 1972; Tester 1973; Jones 1977; Campos & Serrão 1998; Aurégan *et al.* 2001; Vilenski & Rienstra 2007), and it seems a sensible extension of these works to include viscosity without extra complications.

These assumptions are used in § 2 to derive the governing equations, and some facts about their solution are briefly mentioned in § 3. The governing equations are then solved numerically, with some numerical results presented in § 4. The results of a comprehensive study of high- and low-frequency asymptotics are given in § 5, the details of which are in the Appendices. The unbounded temporal growth rate seen by applying the Myers boundary condition to a mass–spring–damper boundary is shown to also occur for the present model in § 6, together with a brief discussion of the effects of this on the mathematical stability of the model. Conclusions are presented in § 7.

https://doi.org/10.1017/jfm.2011.116 Published online by Cambridge University Press

Density	$\rho^* = \rho_0^* \rho$	Pressure & viscous stress	$p^* = c_0^{*2} \rho_0^* p$
Velocity	$\boldsymbol{u}^* = c_0^* \boldsymbol{u}$	Dynamic viscosity (shear & bulk)	$\mu^* = c_0^* \ell^* \rho_0^* \mu$
Distance	$x^* = \ell^* x$	Thermal conductivity	$\kappa^* = c_0^* \ell^* \rho_0^* c_p{}^* \kappa$
Time	$t^* = \ell^*/c_0^* t$	Temperature	$T^* = c_0^{*2}/c_p{}^* T$

TABLE 1. Dimensional and non-dimensional variables, based on a length scale ℓ^*, a velocity c_0^*, a density ρ_0^* and a specific heat at constant pressure $c_p{}^*$. The * denotes a dimensional variable.

2. Governing equations

We consider a compressible viscous perfect gas (a similar derivation is valid for an incompressible fluid). The dimensional and non-dimensional variables used are listed in table 1. Writing $\mathrm{D}/\mathrm{D}t \equiv \partial/\partial t + \boldsymbol{u}\cdot\boldsymbol{\nabla}$, the non-dimensional governing equations are (Landau & Lifshitz 1987)

$$\frac{\partial \rho}{\partial t} + \boldsymbol{\nabla}\cdot(\rho \boldsymbol{u}) = 0, \tag{2.1a}$$

$$\rho \frac{\mathrm{D}\boldsymbol{u}}{\mathrm{D}t} = -\boldsymbol{\nabla} p + \boldsymbol{\nabla}\cdot\sigma, \tag{2.1b}$$

$$\sigma_{ij} = \mu\left(\frac{\partial u_i}{\partial x_j} + \frac{\partial u_j}{\partial x_i}\right) + \left(\mu^B - \frac{2}{3}\mu\right)\delta_{ij}\boldsymbol{\nabla}\cdot\boldsymbol{u}, \tag{2.1c}$$

$$\rho \frac{\mathrm{D}T}{\mathrm{D}t} = \frac{\mathrm{D}p}{\mathrm{D}t} + \sigma_{ij}\frac{\partial u_i}{\partial x_j} + \boldsymbol{\nabla}\cdot(\kappa \boldsymbol{\nabla} T), \tag{2.1d}$$

$$T = \frac{\gamma}{\gamma - 1}\frac{p}{\rho}, \tag{2.1e}$$

where $\gamma = c_p{}^*/c_v{}^*$ is the ratio of specific heats. We assume the viscosity μ, the bulk (or volume) viscosity μ^B and the thermal conductivity κ to depend linearly on temperature and be independent of pressure (Prangsma, Alberga & Beenakker 1973), so that

$$\mu = \frac{T}{T_0 Re}, \quad \mu^B = \frac{T}{T_0 Re}\frac{\mu_0^{B^*}}{\mu_0^*}, \quad \kappa = \frac{T}{T_0 Pr\, Re}, \tag{2.1f}$$

where T_0 is a (non-dimensionalized) reference temperature at which the viscosity is μ_0^*, $\mu_0^{B^*}/\mu_0^*$ is the ratio of bulk to shear viscosity which we assume to be constant, and we have defined $Re = c_0^* \ell^* \rho_0^*/\mu_0^*$ and $Pr = \mu_0^* c_p{}^*/\kappa_0^*$. Re may be interpreted as the Reynolds number and Pr as the Prandtl number, both based on the non-dimensionalization given in table 1. This temperature dependence was not considered by Aurégan *et al.* (2001).

The analysis presented here is valid for flow over a compliant or permeable surface for many geometries. For definiteness, we shall consider here the specific case of flow along a cylindrical tube, as shown in figure 1. The tube is of radius ℓ^* and is parallel to the x^*-axis, with the cross-section described by polar coordinates (r^*, θ). The mean flow consists of a boundary layer of width δ^*, outside which the flow is uniform in the x^*-direction at velocity U_0^*. Within the boundary layer the flow is assumed parallel with u^*, p^*, T^* and ρ^* all functions of radius. The length scale ℓ^* is the radius of the tube, the reference velocity c_0^* is the speed of sound within the uniform flow, and the reference quantities ρ_0^*, T_0^*, μ_0^*, $\mu_0^{B^*}$ and κ_0^* are the values within the uniform flow. This gives $T_0 = 1/(\gamma - 1)$ and $p_0 = 1/\gamma$. The non-dimensionalized uniform-flow velocity $U_0 = M$ is the Mach number. For this cylindrical geometry, using a subscript

https://doi.org/10.1017/jfm.2011.116 Published online by Cambridge University Press

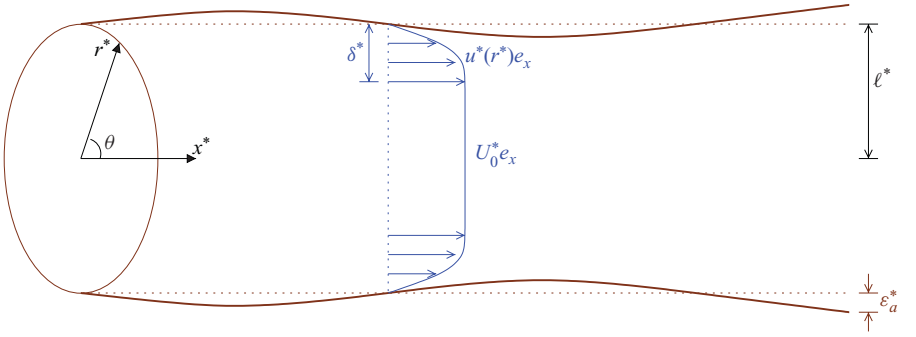


FIGURE 1. (Colour online available on journals.cambridge.org/FLM) Schematic of parallel flow in a cylindrical tube with a coupled boundary.

to denote differentiation, the governing equations (2.1*a*)–(2.1*d*) become

$$\rho_t + (\rho u)_x + \frac{1}{r}(r\rho v)_r + \frac{1}{r}(\rho w)_\theta = 0, \tag{2.2a}$$

$$\rho\left(u_t + uu_x + vu_r + \frac{1}{r}wu_\theta\right) = -p_x + (\sigma_{11})_x + \frac{1}{r}(r\sigma_{12})_r + \frac{1}{r}(\sigma_{13})_\theta, \tag{2.2b}$$

$$\rho\left(v_t + uv_x + vv_r + \frac{1}{r}wv_\theta\right) = \frac{1}{r}\rho w^2 - p_r - \frac{1}{r}\sigma_{33} + (\sigma_{12})_x + \frac{1}{r}(r\sigma_{22})_r + \frac{1}{r}(\sigma_{23})_\theta, \tag{2.2c}$$

$$\rho\left(w_t + uw_x + vw_r + \frac{1}{r}ww_\theta\right) = -\frac{1}{r}\rho vw - \frac{1}{r}p_\theta + (\sigma_{13})_x + \frac{1}{r^2}(r^2\sigma_{23})_r + \frac{1}{r}(\sigma_{33})_\theta, \tag{2.2d}$$

$$\begin{aligned}\rho\left(T_t + uT_x + vT_r + \frac{1}{r}wT_\theta\right) &= \left(p_t + up_x + vp_r + \frac{1}{r}wp_\theta\right) + (\kappa T_x)_x + \frac{1}{r}(r\kappa T_r)_r \\ &+ \frac{1}{r^2}(\kappa T_\theta)_\theta + \sigma_{11}u_x + \sigma_{12}(u_r + v_x) + \sigma_{13}\left(\frac{1}{r}u_\theta + w_x\right) + \sigma_{22}v_r \\ &+ \sigma_{23}\left(\frac{1}{r}v_\theta + r\left(\frac{w}{r}\right)_r\right) + \frac{1}{r}\sigma_{33}(w_\theta + v),\end{aligned} \tag{2.2e}$$

$$\sigma_{ij} = \mu\begin{pmatrix} 2u_x & u_r + v_x & \frac{1}{r}u_\theta + w_x \\ \cdot & 2v_r & \frac{1}{r}v_\theta + r\left(\frac{w}{r}\right)_r \\ \cdot & \cdot & \frac{2}{r}(w_\theta + v)\end{pmatrix} + \left(\mu^B - \frac{2}{3}\mu\right)\left[u_x + \frac{1}{r}(rv)_r + \frac{1}{r}w_\theta\right]\delta_{ij}. \tag{2.2f}$$

Since $\mu_0 = 1/Re \ll 1$, viscosity is assumed to be unimportant within the flow outside the boundary layer, so outside the boundary layer these equations reduce to the inviscid Euler equations. We now change variables to concentrate on the behaviour within the boundary layer. Balancing the viscous and inertial terms gives the boundary-layer scaling

$$r = 1 - \delta y, \quad v = -\delta v_1, \quad \delta^2 = 1/Re. \tag{2.3}$$

https://doi.org/10.1017/jfm.2011.116 Published online by Cambridge University Press

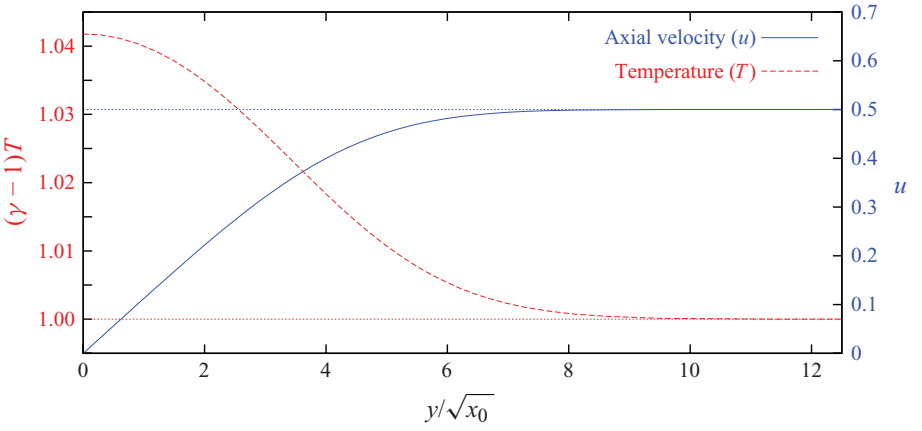


FIGURE 2. (Colour online) Velocity (right scale, solid line) and temperature (left scale, dashed line) for a compressible Blasius boundary layer a distance x_0 downstream of a leading edge. $M = 0.5$, $Pr = 0.7$ and $\gamma = 1.4$.

We now consider solving (2.2) using this scaling, to leading order in δ. First, we shall consider the steady mean flow and then following that small perturbations about this mean flow.

2.1. *Mean flow*

Any boundary-layer profile independent of t, x and θ could be chosen for the analysis that follows. (It should be noted that, in what follows, we have assumed that the fluid and boundary are in thermal equilibrium, so that $T_y(0) = 0$.) Possibilities include 1/7th power law, exponential, logarithmic and quarter sine boundary-layer profiles. We shall take here the axial velocity, pressure and temperature to be that of a compressible Blasius boundary layer a distance x_0 downstream of a leading edge (see, e.g. Schlichting 1968). An example of such a boundary-layer profile is plotted in figure 2. Choosing Re and x_0 allows both the Reynolds number of the outer flow and the displacement thickness of the boundary layer to be set to any desired values.

2.2. *Small perturbations in the boundary layer*

We now consider a small time-dependent perturbation to the steady flow considered above (such perturbations will be denoted by a tilde). We write, for example, $\rho + \tilde{\rho}$ for the density, where ρ is the mean flow and $\tilde{\rho}$ is the perturbation. All perturbations will be of magnitude $\varepsilon_a \ll \delta$ and have dependence $\exp\{\mathrm{i}\omega t - \mathrm{i}kx - \mathrm{i}m\theta\}$.

Outside the boundary layer viscosity is assumed to be unimportant and the mean flow is uniform, so that $\boldsymbol{u} = (M + \tilde{u}_U, \tilde{v}_U, \tilde{w}_U)$, $p = 1/\gamma + \tilde{p}_U$, $\rho = 1 + \tilde{\rho}_U$ and $T = 1/(\gamma - 1) + \tilde{T}_U$. Solving for the perturbation in such a situation is fairly straightforward (e.g. Vilenski & Rienstra 2007; Brambley & Peake 2008), and here we assume that the outer solution is known. We denote $\lim_{r\to 1} \tilde{v}_U = \tilde{v}_\infty$ and $\lim_{r\to 1} \tilde{p}_U = \tilde{p}_\infty$, which will be used to match with the solution within the boundary layer.

Within the boundary layer, we rescale $r = 1 - \delta y$ and set $\boldsymbol{u} = (u + \tilde{u}, -\delta\tilde{v}, \tilde{w})$. Neglecting terms of order $O(\varepsilon_a^2)$ and $O(\delta)$ in the governing equations (2.2*a*)–(2.2*f*)

https://doi.org/10.1017/jfm.2011.116 Published online by Cambridge University Press

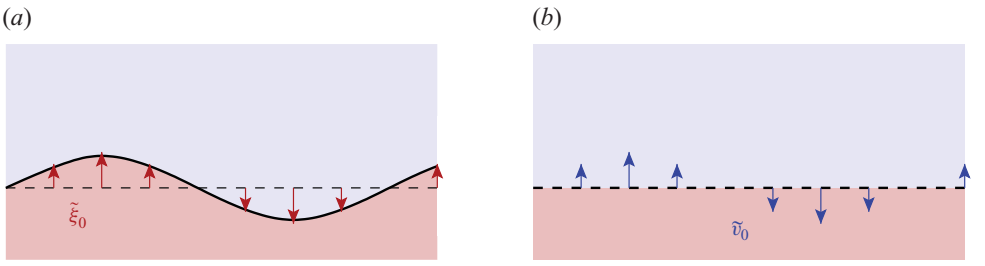


FIGURE 3. (Colour online) Sketches of a compliant (*a*) and a permeable (*b*) boundary. The arrows indicate normal displacement $\tilde{\xi}_0$ in (*a*) and normal velocity $\tilde{v}_0$ in (*b*).

gives

$$\mathrm{i}(\omega - uk)\tilde{p} + \rho(\tilde{v}_y - \mathrm{i}k\tilde{u} - \mathrm{i}m\tilde{w}) + \rho_y\tilde{v} = 0, \tag{2.4a}$$

$$\mathrm{i}(\omega - uk)\tilde{u} + \tilde{v}u_y = \frac{1}{\rho}\mathrm{i}k\tilde{p} + \frac{\gamma - 1}{\rho}(T\tilde{u}_y + \tilde{T}u_y)_y, \tag{2.4b}$$

$$\tilde{p}_y = O(\delta^2), \tag{2.4c}$$

$$\mathrm{i}(\omega - uk)\rho\tilde{w} = \mathrm{i}m\tilde{p} + (\gamma - 1)(T\tilde{w}_y)_y, \tag{2.4d}$$

$$\mathrm{i}(\omega - uk)\tilde{T} + \tilde{v}T_y = \frac{1}{\rho}\mathrm{i}(\omega - uk)\tilde{p} + \frac{\gamma - 1}{\rho Pr}(\tilde{T}T_y + T\tilde{T}_y)_y + \frac{(\gamma - 1)}{\rho}(\tilde{T}(u_y)^2 + 2Tu_y\tilde{u}_y), \tag{2.4e}$$

$$(\gamma - 1)\rho^2\tilde{T} = \gamma\rho\tilde{p} - \tilde{\rho}. \tag{2.4f}$$

Hence, $\tilde{p}$ is constant across the boundary layer to leading order. Since the curvature of the cylindrical boundary occurs at $O(\delta)$, the above equations are equally valid for a flat surface.

Matching the boundary-layer perturbation with the perturbation in the uniform flow gives $\tilde{p}$ and $\tilde{w}$ being $O(1)$, while $\tilde{u}$, $\tilde{v}$, $\tilde{\rho}$ and $\tilde{T}$ are $O(1/\delta)$ owing to matching $\tilde{v}_\infty$ with $-\delta\tilde{v}$. These assumptions give, to leading order, $\tilde{\rho} = -(\gamma - 1)\rho^2\tilde{T}$ and

$$\mathrm{i}(\omega - uk)\tilde{T} + T_y\tilde{v} - T\tilde{v}_y + \mathrm{i}kT\tilde{u} = 0, \tag{2.5a}$$

$$\mathrm{i}(\omega - uk)\tilde{u} + \tilde{v}u_y = (\gamma - 1)^2T(T\tilde{u}_y + \tilde{T}u_y)_y, \tag{2.5b}$$

$$\mathrm{i}(\omega - uk)\tilde{T} + \tilde{v}T_y = (\gamma - 1)^2T\left[\frac{1}{Pr}(\tilde{T}T)_{yy} + \tilde{T}(u_y)^2 + 2Tu_y\tilde{u}_y\right]. \tag{2.5c}$$

If the fluid is incompressible, the nonlinear equations of motion (2.1) must be modified. It turns out that the linear equations of motion (2.5*a*) and (2.5*b*) remain valid for an incompressible fluid, provided we take $T(y) \equiv 1/(\gamma - 1)$ and $\tilde{T} = 0$ irrespective of the actual temperature of the incompressible fluid.

2.3. *The fluid–solid boundary condition*

We now considered the boundary conditions to the boundary-layer perturbation equation (2.5) derived above. Two types of boundaries will be considered here, as shown in figure 3. The term *compliant boundary* will be used for a boundary which may be deformed by the fluid but is impermeable, as shown in figure 3(*a*). If the velocity of the boundary is $(\tilde{u}_0, \tilde{v}_0, \tilde{w}_0)$ at (x_0, θ_0) and the temperature of the boundary

https://doi.org/10.1017/jfm.2011.116 Published online by Cambridge University Press

is $T(0)+\tilde{T}_0$, then rescaling to within the boundary layer means we require

$$\left.\begin{aligned} T(y)+\tilde{T}(x+\tilde{x},y,\theta+\tilde{\theta}) &= \tilde{T}_0(x,\theta)+T(0)\\ u(y)+\tilde{u}(x+\tilde{x},y,\theta+\tilde{\theta}) &= \tilde{u}_0(x,\theta)\\ \tilde{v}(x+\tilde{x},y,\theta+\tilde{\theta}) &= -\tilde{v}_0(x,\theta)/\delta\\ \tilde{w}(x+\tilde{x},y,\theta+\tilde{\theta}) &= \tilde{w}_0(x,\theta)\end{aligned}\right\} \quad \text{at } y=-\tilde{\xi}_0/\delta, \tag{2.6}$$

where $\tilde{\xi}_0=\tilde{v}_0/(\mathrm{i}\omega)$ is the normal displacement of the wall in the radial direction, and $\tilde{x}=\tilde{u}_0/(\mathrm{i}\omega)$ and $\tilde{\theta}=\tilde{w}_0/(\mathrm{i}\omega)$ are the tangential displacements of the wall. Linearizing and taking only the leading-order terms, which are of order $1/\delta$, gives the boundary conditions

$$\left.\begin{aligned} \tilde{u}(0) &= Cu_y(0)\frac{\tilde{v}_0/\delta}{\mathrm{i}\omega}, \quad \tilde{v}(0) = -\tilde{v}_0/\delta, \quad \tilde{T}(0)=0,\\ \tilde{u}(y) &\to 0, \qquad\qquad \tilde{v}(y)\to -\tilde{v}_\infty/\delta, \quad \tilde{T}(y)\to 0, \quad \text{as } y\to\infty,\end{aligned}\right\} \tag{2.7}$$

with $C=1$, the 'C' standing for 'compliant'.

In contrast, we will use the term *permeable boundary* for a boundary which remains fixed at $y=0$ and through which the fluid may flow, as shown in figure 3(b). For such a boundary, the boundary conditions are

$$\tilde{u}(x,0,\theta)=0, \quad \tilde{v}(x,0,\theta)=-\tilde{v}_0(x,\theta)/\delta, \quad \tilde{w}(x,0,\theta)=0. \tag{2.8}$$

This gives the same boundary conditions as (2.7) but with $C=0$.

2.4. *Impedance models of the boundary*

The boundary reacts to the disturbance in the fluid, linking the wall pressure $\tilde{p}_0$ and the wall velocity $(\tilde{u}_0,\tilde{v}_0,\tilde{w}_0)$. The boundary *impedance* is given by $Z=\tilde{p}_0/\tilde{v}_0$.

Given the impedance of the boundary, we would like to know the effective impedance $Z_{eff}=\tilde{p}_\infty/\tilde{v}_\infty$ seen by the inviscid perturbation to the mean flow above the boundary layer. Since pressure is constant throughout the boundary layer to leading order, so that $\tilde{p}_0=\tilde{p}=\tilde{p}_\infty$, Z_{eff} is given by

$$Z_{eff}=Z\frac{\tilde{v}_0}{\tilde{v}_\infty}. \tag{2.9}$$

Neglecting viscous dissipation in the boundary layer, the normal particle displacement $\tilde{\xi}$ would be constant across the boundary layer (Eversman & Beckemeyer 1972; Tester 1973), so that $\tilde{v}_0=\mathrm{i}\omega\tilde{\xi}$, $\tilde{v}_\infty=\mathrm{i}(\omega-Mk)\tilde{\xi}$, and therefore

$$Z_{eff}=\frac{Z}{1-Mk/\omega}. \tag{2.10}$$

This is referred to here as *continuity of displacement*, and we set $Z_{disp}=Z/(1-Mk/\omega)$. This boundary condition is often referred to as the Myers boundary condition (Myers 1980). Aurégan *et al.* (2001) predicted this to hold in the high-frequency limit.

In the low-frequency limit, Aurégan *et al.* (2001) predicted mass flux, $\rho\tilde{v}$, to be constant through the boundary layer. Assuming this gives the effective impedance as

$$Z_{eff}=Z(\gamma-1)T(0). \tag{2.11}$$

This is referred to here as *continuity of mass flux*, and we set $Z_{mass}=Z(\gamma-1)T(0)$.

To summarize, the leading-order equations for a linearized perturbation to a thin parallel boundary layer are (2.5), subject to the boundary conditions (2.7). We are

https://doi.org/10.1017/jfm.2011.116 Published online by Cambridge University Press

interested in $\tilde{v}_\infty/\tilde{v}_0$, as this gives the effective impedance of the boundary as seen by the uniform-flow perturbation outside the boundary layer.

3. Implications of the governing equations

We now note two important consequences of the governing equations (2.5) and boundary conditions (2.7): a branch cut caused by the boundary conditions (§ 3.1) and the effect of rescaling the size of the boundary layer (§ 3.2).

3.1. *The boundary-layer solution outside the boundary layer*

Consider the boundary-layer solution as $y \to \infty$. We assume that, sufficiently far from the boundary, the mean boundary-layer velocity, temperature and pressure attain their uniform-flow values, so that for some Y, $u(y) = M$ and $T(y) = 1/(\gamma - 1)$ for $y > Y$. This is true for practical purposes (computational precision being about 10^{-16}) for the Blasius boundary layer shown in figure 2 for $Y \gtrsim 12\sqrt{x_0}$. In this region, the governing equations within the boundary layer (2.5) simplify and uncouple to give

$$\mathrm{i}(\omega - Mk)(\gamma - 1)\tilde{T} + \mathrm{i}k\tilde{u} = \tilde{v}_y, \tag{3.1a}$$

$$\mathrm{i}(\omega - Mk)\tilde{u} = \tilde{u}_{yy}, \tag{3.1b}$$

$$\mathrm{i}(\omega - Mk)\tilde{T} = \frac{1}{Pr}\tilde{T}_{yy}. \tag{3.1c}$$

with the solutions that are bounded as $y \to \infty$ given by

$$\left.\begin{aligned} \tilde{u}(y) = \tilde{u}_\infty \exp\{-\eta_\infty y\}, \quad \tilde{T}(y) = \tilde{T}_\infty \exp\{-\sigma\eta_\infty y\}, \\ \tilde{v}(y) = \tilde{v}_\infty - \frac{\eta_\infty(\gamma-1)}{\sigma}\tilde{T}_\infty \exp\{-\sigma\eta_\infty y\} - \frac{\mathrm{i}k}{\eta_\infty}\tilde{u}_\infty \exp\{-\eta_\infty y\}, \\ \sigma = +\sqrt{Pr}, \quad \eta_\infty = \sqrt{\mathrm{i}(\omega - Mk)} \quad \text{with} \quad \mathrm{Re}\,\eta_\infty > 0. \end{aligned}\right\} \tag{3.2}$$

This exact solution for $y > Y$ may be used to give a numerical boundary condition at $y = Y$, rather than having to integrate numerically to $y = \infty$. This is discussed further in § 4. From the definition of η_∞, there is a branch cut when $\mathrm{i}(\omega - Mk)$ is both real and negative. For fixed ω, this gives a branch cut in the k-plane along $k = \omega/M - \mathrm{i}q$ for $q \geqslant 0$. This branch cut is different from a critical layer, which is a singularity at $y = y_0$ in the inviscid Pridmore–Brown equations where $\omega - u(y_0)k = 0$; critical layers would be expected for the values of ω and k for which $(\omega - Mk) = -q$ for $q \geqslant 0$. Viscosity regularizes the critical layer singularity, as is shown for our boundary-layer approximation (2.5) using a Frobenius expansion in Appendix A.

3.2. *The effect of boundary-layer thickness*

Throughout this paper, all examples presented are for boundary thicknesses corresponding to $x_0 = 1$. In fact, these results are universal, with the only effect of changing x_0 being to rescale ω, k, $\tilde{u}$, $\tilde{T}$ and y. Suppose $\tilde{u}_1(y)$, $\tilde{T}_1(y)$ and $\tilde{v}_1(y)$ are the solution to the governing equations (2.5) and boundary conditions (2.7) for a boundary-layer profile given by $u_1(y)$ and $T_1(y)$ for parameters $\omega_1 = x_0\omega$ and $k_1 = x_0 k$. Then the solution to the governing equations and boundary conditions for a boundary-layer profile given by $u(y) = u_1(y/\sqrt{x_0})$ and $T(y) = T_1(y/\sqrt{x_0})$ for parameters ω and k is given by

$$\tilde{u}(y) = \sqrt{x_0}\tilde{u}_1(y/\sqrt{x_0}), \quad \tilde{T}(y) = \sqrt{x_0}\tilde{T}_1(y/\sqrt{x_0}), \quad \tilde{v}(y) = \tilde{v}_1(y/\sqrt{x_0}), \tag{3.3}$$

as can be verified by direct substitution. This shows that the behaviour for $x_0 = 1$ is universal.

https://doi.org/10.1017/jfm.2011.116 Published online by Cambridge University Press

4. Numerical results

Having derived the mathematical model we will be considering in § 2 and noted some properties of this model in § 3, in this section (2.5) is solved numerically and some numerical results are presented. The equations were solved numerically using a fourth-order symmetric finite difference scheme on an equally spaced set of N points in the interval $y \in [0, Y]$, yielding a $3N \times 3N$ banded matrix $\boldsymbol{A}$ with at most $48N$ non-zero elements. The boundary conditions at $y = 0$ were specified as in (2.7) with $\tilde{v}_0 = -\delta$. For the boundary condition at $y = \infty$, the analytic solutions for $y > Y$ from (3.2) were used to give the numerical boundary conditions at $y = Y$:

$$\tilde{u}_y + \eta_\infty \tilde{u} = 0, \quad \tilde{T}_y + \sigma \eta_\infty \tilde{T} = 0. \tag{4.1}$$

These boundary conditions were encapsulated into a $3N$-dimensional vector $\boldsymbol{b}$, with $b_1 = 1$ and $b_i = 0$, $i \in [2, 3N]$. The discretized problem was therefore to solve $\boldsymbol{Ax} = \boldsymbol{b}$ for the solution $\boldsymbol{x}$, which was performed using the LAPACK ZGBSV routine (Anderson *et al.* 1999). After this calculation, (3.2) was used to extrapolate $\tilde{v}(Y)$ to $\tilde{v}(\infty) = \tilde{v}_\infty$. Typically, $Y = 16\sqrt{x_0}$ and $N = 4000$ were used for the results that follow, with each solution taking about 10 ms on a standard desktop computer. Checks were performed in each case to ensure that these parameters were sufficient, by verifying that the solution remained unaltered by increasing N and by verifying the numerical solution against the analytic solution (3.2) for $y > Y$.

We now consider the effect of the viscous boundary layer on the response of the boundary at high (§ 4.1) and low (§ 4.2) frequencies, and the resulting effect of this on acoustic modes in a cylindrical lined duct (§ 4.3).

4.1. *High-frequency results*

At high frequency, we would expect from Aurégan *et al.* (2001) that $Z_{eff} = Z_{disp}$; i.e. the Myers boundary condition should hold. The variation of Z_{eff}/Z_{disp} in the k-plane, calculated numerically for $\omega = 31$, $\gamma = 1.4$, $Pr = 0.7$, $M = 0.5$ and $x_0 = 1$ (intended to be typical of tonal fan noise within an aeroengine intake), is shown in figure 4. For a compliant boundary (figure 4*a*,*b*), as expected, $Z_{eff}/Z_{disp} \approx 1$ to a reasonably good accuracy for the majority of the k-plane. The branch cut mentioned in § 3.1 is just about visible, extending in the negative imaginary direction from $k = \omega/M = 62$. For a permeable boundary (figure 4*c*,*d*), $Z_{eff}/Z_{disp} \approx 1$ in the upper and left halves of the k-plane. The branch cut is clearly visible in this case, beyond which is an anomalous region where it is clearly not true that $Z_{eff}/Z_{disp} \approx 1$. This behaviour was not seen by Aurégan *et al.* (2001), since they considered only the limit of a low flow speed for which the branch cut is at infinity.

4.2. *Low-frequency results*

At low frequencies, plots of Z_{eff}/Z_{disp} show that continuity of displacement does not hold for either compliant or permeable boundaries for $\omega \ll 1$. Aurégan *et al.* (2001) suggest that at low frequencies we should expect $Z_{eff} \approx Z_{mass}$. The variation of Z_{eff}/Z_{mass} in the k-plane, calculated for the same parameters as in figure 4 but with $\omega = 0.03$, is shown in figure 5. For a permeable boundary ($C = 0$, figure 5*c*,*d*), arguably $Z_{eff}/Z_{mass} \approx 1$ is a good approximation for the majority of the k-plane, at least away from the point $k = \omega/M$. However, continuity of mass flux does not appear correct for the compliant boundary ($C = 1$, figure 5*a*,*b*); this may be seen especially by comparing figures 5(*b*) and 5(*d*), which show the permeable boundary maintaining $\arg(Z_{eff}/Z_{mass})$ within about $\pm\pi/8$, while the compliant boundary has $\arg(Z_{eff}/Z_{mass})$ varying beyond $3\pi/4$ even outside the anomalous region and away

https://doi.org/10.1017/jfm.2011.116 Published online by Cambridge University Press

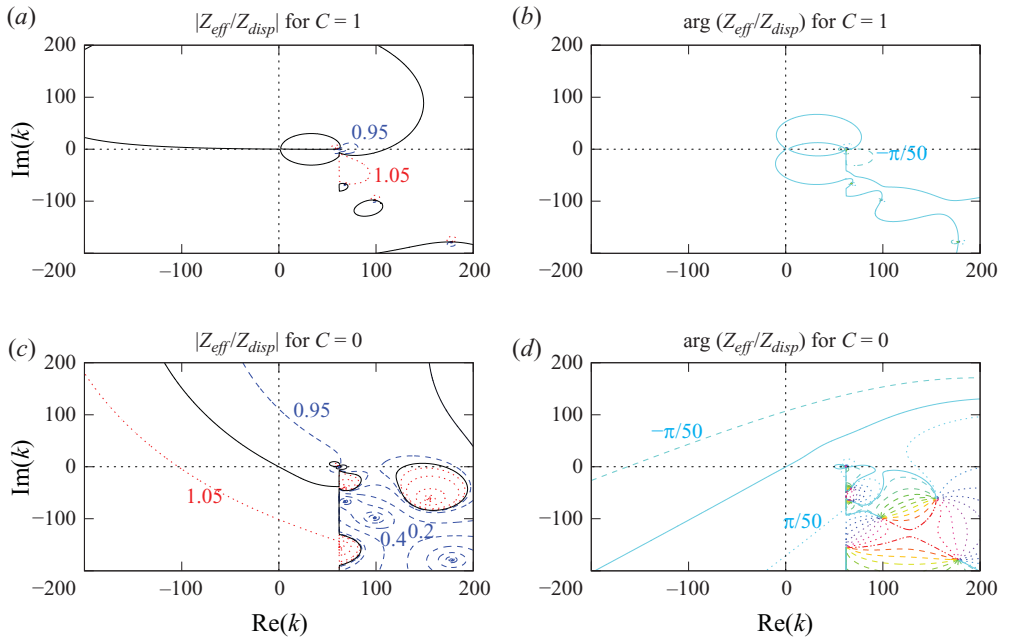


FIGURE 4. (Colour online) Contours of Z_{eff}/Z_{disp} in the k-plane at high frequency. For (a) and (c), contours are of $|Z_{eff}/Z_{disp}|$; the solid, dashed and dotted lines are for $= 1$, <1 and >1, respectively, spaced logarithmically. For (b) and (d), contours are for $\arg(Z_{eff}/Z_{disp})$; the solid, dashed, dotted and dash-dotted lines are for $= 0$, $\in (0, \pi)$, $\in (-\pi, 0)$ and $= \pi$, respectively. $\omega = 31$, $Pr = 0.7$, $\gamma = 1.4$, $M = 0.5$ and $x_0 = 1$.

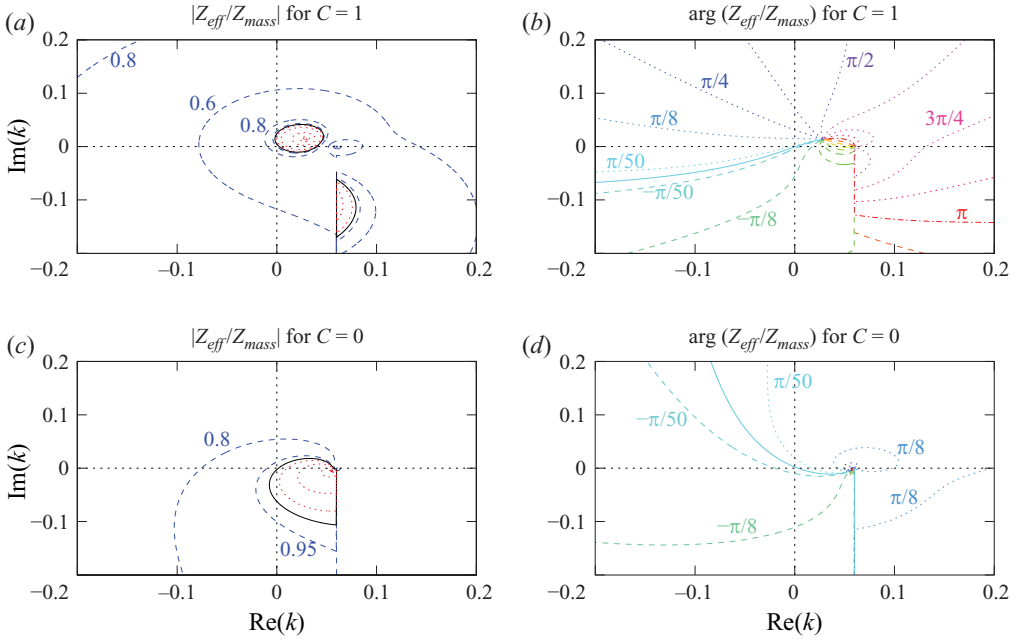


FIGURE 5. (Colour online) Contours of Z_{eff}/Z_{mass} in the k-plane at low frequency. For (a) and (c), contours are of $|Z_{eff}/Z_{mass}|$; the solid, dashed and dotted lines are for $= 1$, <1 and >1, respectively, spaced logarithmically. For (b) and (d), contours are of $\arg(Z_{eff}/Z_{mass})$; the solid, dashed, dotted and dash-dot lines are for $= 0$, $\in (0, \pi)$, $\in (-\pi, 0)$, and $= \pi$, respectively. $\omega = 0.03$, $Pr = 0.7$, $\gamma = 1.4$ and $M = 0.5$, $x_0 = 1$.

https://doi.org/10.1017/jfm.2011.116 Published online by Cambridge University Press

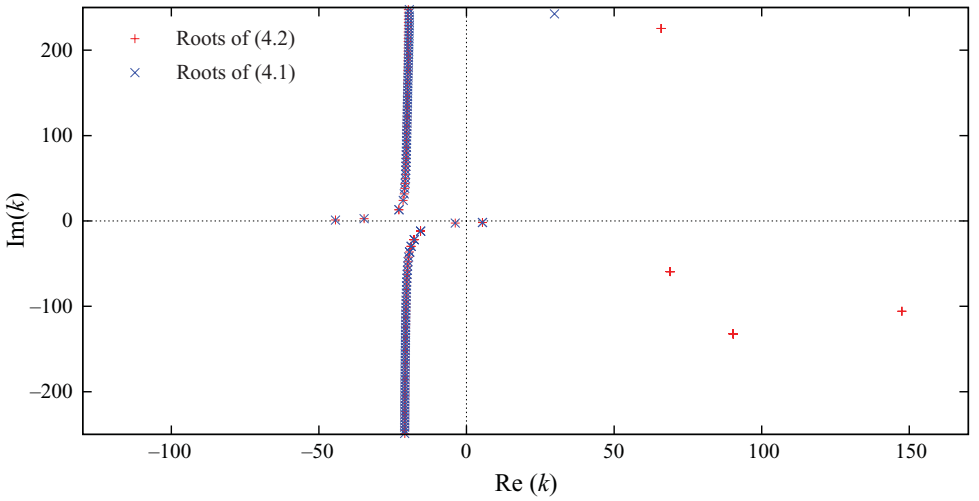


FIGURE 6. (Colour online) Modes in the k-plane for a cylindrical duct, using the boundary-layer boundary condition (+, 4.5) and the continuity of displacement boundary condition (×, 4.4). $Z = 2 + \mathrm{i}$, $\omega = 31$, $m = 24$, $M = 0.5$, $Pr = 0.7$, $\gamma = 1.4$ and $x_0 = 1$.

from $k = \omega/M$. This difference becomes more obvious for even smaller frequencies and will be investigated further using asymptotics in § 5.2.

4.3. *Effect of the boundary layer on acoustic duct modes*

Having looked at the effect of the boundary layer on the behaviour of the boundary, we now investigate its effect on the acoustic modes in a cylindrical lined duct. Consider acoustic waves in a cylindrical duct with uniform flow and a permeable boundary (e.g. Rienstra 2003), with solution

$$\tilde{\boldsymbol{u}}_U = \nabla\phi, \quad \phi = A\mathrm{J}_m(\alpha r)\exp\{\mathrm{i}\omega t - \mathrm{i}kx - \mathrm{i}m\theta\}, \tag{4.2}$$

$$\tilde{p}_U = \tilde{\rho}_U = -\mathrm{i}(\omega - Mk)\phi, \quad \alpha^2 = (\omega - Mk)^2 - k^2, \tag{4.3}$$

where J_m are the Bessel functions of the first kind. Assuming continuity of displacement (the Myers boundary condition), the boundary condition at $r = 1$ gives the dispersion relation

$$1 - \frac{(\omega - Mk)^2}{\mathrm{i}\omega Z}\frac{\mathrm{J}_m(\alpha)}{\alpha \mathrm{J}_m'(\alpha)} = 0. \tag{4.4}$$

Accounting for the boundary layer using (2.5) gives the dispersion relation

$$1 + \frac{\mathrm{i}(\omega - Mk)}{Z\tilde{v}_0/\tilde{v}_\infty}\frac{\mathrm{J}_m(\alpha)}{\alpha \mathrm{J}_m'(\alpha)} = 0. \tag{4.5}$$

Figure 6 shows the effect of the boundary layer on these duct modes for a permeable boundary. The acoustic modes, both cut-on and cut-off, are identical for both boundary conditions. The potential hydrodynamic instability mode (Rienstra 2003; Brambley & Peake 2006) in the upper-right quadrant is noticeably different for the two boundary conditions. Moreover, in the lower-right quadrant there are three boundary-layer modes with no uniform-flow equivalent. These three modes are in the anomalous region seen in figure 4 and disappear behind the branch cut as $\mathrm{Im}(\omega) \to -\infty$.

https://doi.org/10.1017/jfm.2011.116 Published online by Cambridge University Press

5. Asymptotics

In this section, some asymptotic predictions are made to explain and understand some of the features seen in the numerical examples in the previous section. We rescale $\tilde{u}$, $\tilde{v}$ and $\tilde{T}$ by $-\tilde{v}_0/\delta$, so that the governing equations (2.5) remain the same while the boundary conditions (2.7) become

$$\left.\begin{array}{lll} \tilde{u}(0) = -C\dfrac{u_y(0)}{\mathrm{i}\omega}, & \tilde{v}(0) = 1, & \tilde{T}(0) = 0, \\ \tilde{u}(y) \to 0, & \tilde{v}(y) \to \tilde{v}_\infty/\tilde{v}_0, & \tilde{T}(y) \to 0, \quad \text{as} \quad y \to \infty. \end{array}\right\} \tag{5.1}$$

The quantity $\tilde{v}_\infty/\tilde{v}_0$ is the unknown we would like to calculate. We will be interested in asymptotic solutions to this set of equations in the low- (§§ 5.1 and 5.2) and high-frequency (§ 5.3) limits with $k/\omega = O(1)$. The details of the derivation of these results are given in the Appendices.

5.1. *Low frequencies for permeable boundaries*

Consider the behaviour of $\tilde{v}_\infty/\tilde{v}_0$ in the low-frequency limit $\omega \ll 1$ with $\omega/k = O(1)$ for a permeable boundary. After some algebra (given in Appendix B), we find that

$$\frac{\tilde{v}_\infty}{\tilde{v}_0} = \frac{1}{(\gamma-1)T(0)} + \omega^{1/2}\sqrt{\mathrm{i}(1-Mk/\omega)}\left[\frac{(\gamma-1)}{\sqrt{Pr}}F(\infty) + \frac{A}{\omega/k - M}\right] + O(\omega), \tag{5.2}$$

where

$$\frac{1}{Pr}(TF)_{yy} - (u_y)^2 F = \frac{T_y + 2u_y(M-u)}{(\gamma-1)^2 T(0)}, \quad \text{with } F(0) = F_y(\infty) = 0, \tag{5.3}$$

$$A = \int_0^\infty \frac{u(y) - M}{(\gamma-1)^2 T(0) T(y)} - \frac{F(y)u_y(y)}{T(y)}\,\mathrm{d}y. \tag{5.4}$$

To leading order this is the continuity of mass flux across the boundary layer, agreeing with Aurégan *et al.* (2001). The first-order correction at $O(\omega^{1/2})$ is in terms of the integrals of the mean-flow velocity and temperature profiles. These asymptotics have been verified against the numerics for numerous values of all parameters, some of which are plotted in Appendix B.

5.2. *Low frequencies for compliant boundaries*

The low-frequency asymptotics for compliant and permeable boundaries are significantly different, since the $\tilde{u}$ boundary condition (2.7) implies $\tilde{u} = O(1/\omega)$ for a compliant boundary. In this case, after a different asymptotic analysis (given in Appendix C), we find

$$\frac{\tilde{v}_\infty}{\tilde{v}_0} = -\omega^{-1/2}\frac{u_y(0)k/\omega}{\sqrt{\mathrm{i}(1-Mk/\omega)}} + (1-Mk/\omega)\frac{u_y(0)f(\infty)}{\sqrt{Pr}} - \frac{ku_y(0)}{\omega}\int_0^\infty \frac{u_y(y)f(y)}{(\gamma-1)T(y)}\,\mathrm{d}y + \frac{1}{(\gamma-1)T(0)} + O(\sqrt{\omega}), \tag{5.5}$$

where

$$\frac{1}{Pr}(Tf)_{yy} - (u_y)^2 f = -2u_y, \quad \text{with } f(0) = f_y(\infty) = 0. \tag{5.6}$$

The first term in (5.5) is the direct effect of the compliant boundary. The second and third terms are the indirect effect of the compliant boundary acting through the temperature, and are not present for an incompressible fluid. The final term in (5.5) is the continuity of the mass flux term, as for a permeable boundary. This demonstrates

https://doi.org/10.1017/jfm.2011.116 Published online by Cambridge University Press

a major difference between a compliant and a permeable boundary, since $\tilde{v}_\infty/\tilde{v}_0$ are of different orders of magnitude in each case.

5.3. *High frequencies and short wavelengths*

Consider solving the governing equations (2.5) in the the high-frequency limit $\omega \gg 1$ with $k/\omega \leqslant O(1)$. The details for this, together with the short-wavelength case ($k \gg 1$ with $\omega/k \leqslant O(1)$), are given in Appendix D. We use the method of multiple scales (see, e.g. Hinch 1991), introducing a fast variable $\theta(y)$ such that

$$\theta(y) = \omega^{-1/2}\int_0^y \bar{\eta}(y')\,\mathrm{d}y', \quad \mathrm{Re}(\omega^{1/2}) > 0, \tag{5.7}$$

$$\bar{\eta}(y)^2 = \frac{\mathrm{i}(1-u(y)k/\omega)}{(\gamma-1)^2T(y)^2}, \quad \mathrm{Re}(\bar{\eta}(y)) > 0 \quad \text{as } y \to \infty. \tag{5.8}$$

We shall assume that $\bar{\eta}(y) \neq 0$ for any y (otherwise a caustic is present, as dealt with in § D.1). For a compliant boundary, we find

$$\left.\begin{gathered}\tilde{v} = 1 - uk/\omega + O(\omega^{-1}), \quad \tilde{u} = \mathrm{i}u_y/\omega + O(\omega^{-2}), \quad \tilde{T} = \mathrm{i}T_y/\omega + O(\omega^{-2}),\\ Z_{eff} = \frac{Z}{1-Mk/\omega} + O(\omega^{-1}),\end{gathered}\right\} \tag{5.9}$$

while for a permeable boundary,

$$\left.\begin{aligned}\tilde{v} &= \left(1-\frac{uk}{\omega}\right)\left[1+\frac{ku_y(0)}{\omega^{3/2}\bar{\eta}(0)}\right] - \frac{ku_y(0)}{\omega^{3/2}\bar{\eta}}\left(1-\frac{uk}{\omega}\right)^{-3/4}\mathrm{e}^{-\theta} + O(\omega^{-1}),\\ \tilde{u} &= \frac{\mathrm{i}u_y}{\omega} - \frac{\mathrm{i}u_y(0)}{\omega}\left(1-\frac{uk}{\omega}\right)^{-3/4}\mathrm{e}^{-\theta} + O(\omega^{-3/2}), \quad \tilde{T} = \frac{\mathrm{i}T_y}{\omega} + O(\omega^{-3/2}),\\ Z_{eff} &= \frac{Z}{1-Mk/\omega}\left[1-\frac{u_y(0)k}{\bar{\eta}(0)\omega^{3/2}}\right] + O(\omega^{-1}).\end{aligned}\right\} \tag{5.10}$$

To leading order, both of these are continuity of displacement, agreeing with Aurégan *et al.* (2001). These asymptotic results break down in the anomalous region; however, outside this region the asymptotic results have been verified against numerical results for numerous values of all parameters, a selection of which is plotted in Appendix D.

As an example of the breakdown of the asymptotics in the anomalous region, figure 7 compares the numerical results and the asymptotic prediction of (5.10) for a permeable boundary at the moderate frequency $\omega = 31$, for $k = 70\text{–}70\mathrm{i}$, which is in the anomalous region. The asymptotics are obviously getting the wrong result, as is particularly noticeable from the solution at large y. The period and magnitude of the oscillations around $y \in [2, 10]$ are of the correct type, suggesting that the choice of a fast variable θ is still correct. The reason for the dramatic increase in amplitude of the asymptotics is that $\mathrm{Re}(\bar{\eta}(y))$ changes sign, so that initially $\mathrm{e}^{-\theta}$ grows for small y as y increases, before eventually decaying as $y \to \infty$ by the choice of branch of $\bar{\eta}(y)$. This causes the asymptotic analysis to break down, since $\mathrm{e}^{-\theta}$, which was assumed to be at most $O(1)$, may now be exponentially large. The similarity of the period and magnitude of oscillations between the asymptotics and numerics suggests that a similar asymptotic analysis might predict the behaviour within this region, though this is not attempted here.

For $\mathrm{Re}(\bar{\eta}(y))$ to change sign, there must be a value of y for which $\mathrm{Re}(\bar{\eta}(y)) = 0$, implying that $\mathrm{i}(\omega - u(y)k)$ must be real and negative for some y. For real ω, this will happen for some y if and only if $\mathrm{Im}(k) < 0$ and $\mathrm{Re}(k) > \omega/M$. This is exactly the region

https://doi.org/10.1017/jfm.2011.116 Published online by Cambridge University Press

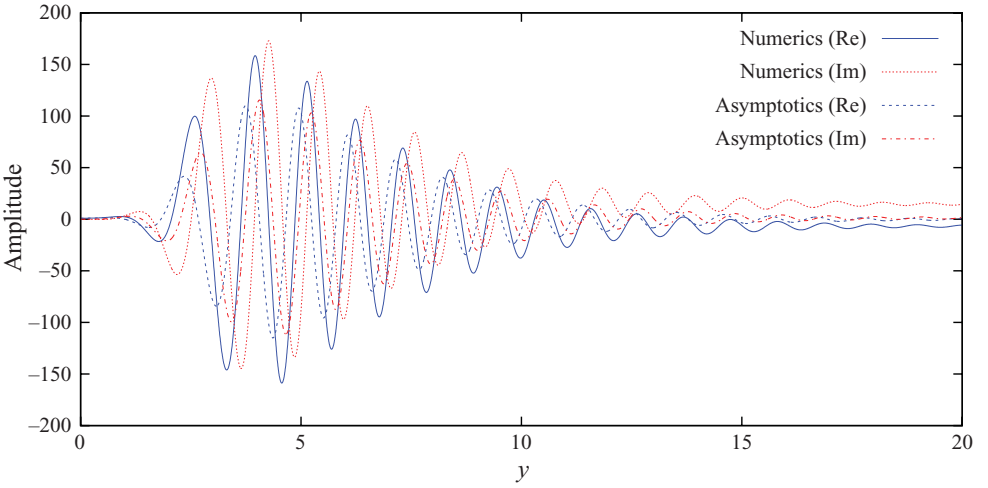


FIGURE 7. (Colour online) Comparison of $\tilde{v}(y)$ calculated numerically against the asymptotics (5.10) for a value of k in the anomalous region. The amplitude is normalized such that $\tilde{v}(y) = 1$ at $y = 0$. $\omega = 31$, $k = 70–70\mathrm{i}$, $M = 0.5$, $Pr = 0.7$, $C = 0$, $\gamma = 1.4$ and $x_0 = 1$.

seen in figure 4 with anomalous behaviour. Provided we are outside this anomalous region, the $\mathrm{e}^{-\theta}$ term is $O(1)$, and the asymptotics above holds. This anomalous region is therefore bounded by the branch cut mentioned above, for which $\mathrm{Re}(k) = \omega/M$, and by the caustic for which $\bar{\eta}(y) = 0$ for some y.

6. Stability

We now show that the viscous-boundary-layer analysis given here leads to similar ill-posedness to compressible slipping flow over a lining modelled using the Myers boundary condition. Illposedness is shown by demonstrating an unbounded temporal growth rate; that is, solving the dispersion relation for ω as a function of k shows that, for real k, $\mathrm{Im}(\omega) \to -\infty$ as $k \to \pm\infty$ for at least one mode (see Brambley 2009, for details).

Figure 8(b) compares $\mathrm{Im}(\omega(k))$ for a mass–spring–damper boundary with impedance of the form $Z = R + \mathrm{i}a\omega - \mathrm{i}b/\omega$ (where $a > 0$ is the mass constant, $b > 0$ is the spring constant and $R > 0$ is the damping constant) using both the Myers continuity of displacement boundary condition from (4.4) and the numerically calculated boundary-layer boundary condition from (4.5). As can be seen, both demonstrate something like $\mathrm{Im}(\omega) = O(k^{1/2})$ behaviour, as is to be expected for (4.4) (Rienstra & Peake 2005; Brambley 2009). The dispersion relation for surface modes (Rienstra 2003; Brambley & Peake 2006) is

$$\sqrt{k^2 + m^2 - (\omega - Mk)^2} + \frac{\mathrm{i}(\omega - Mk)}{Z_{eff}} = 0, \tag{6.1}$$

with $\mathrm{Re}(\sqrt{\cdots}) > 0$. Motivated by the scaling $\omega = O(k^{1/2})$, we consider a caustic at the wall (§ D.1.2, low-$\bar{\omega}$ limit), giving

$$Z_{eff} = Z\frac{0.777\,\mathrm{e}^{\mathrm{i}\pi/6}((\gamma - 1)u_y(0)T(0))^{2/3}}{Mk^{1/3}} \tag{6.2}$$

https://doi.org/10.1017/jfm.2011.116 Published online by Cambridge University Press

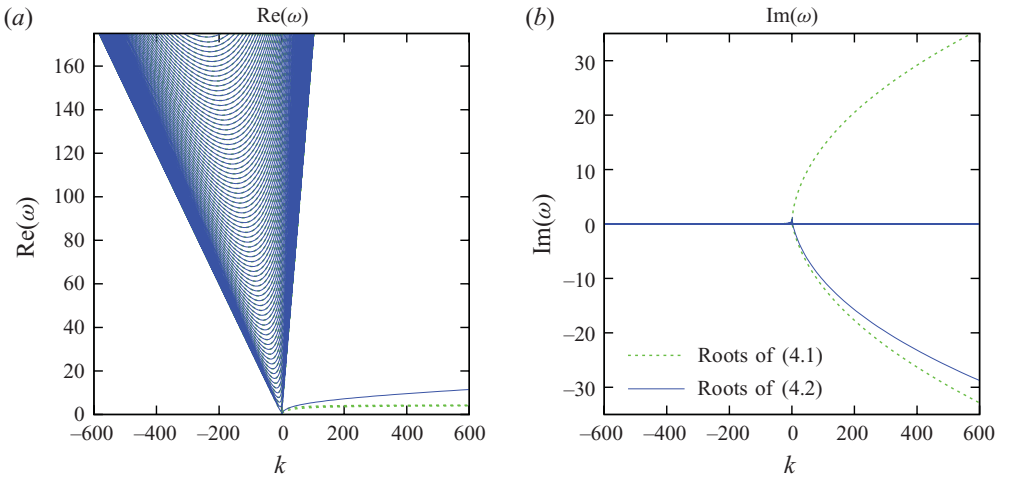


FIGURE 8. (Colour online) Trajectories of $\omega(k)$ as k is varied, for a cylindrical duct with a mass–spring–damper boundary with $Z = 1 + \mathrm{i}(0.335\omega - 0.15/\omega)$. $M = 0.7$, $m = 0$, $Pr = 0.7$ and $x_0 = 1$. Only modes with $\mathrm{Re}(\omega) > 0$ are plotted; the others may be obtained by symmetry.

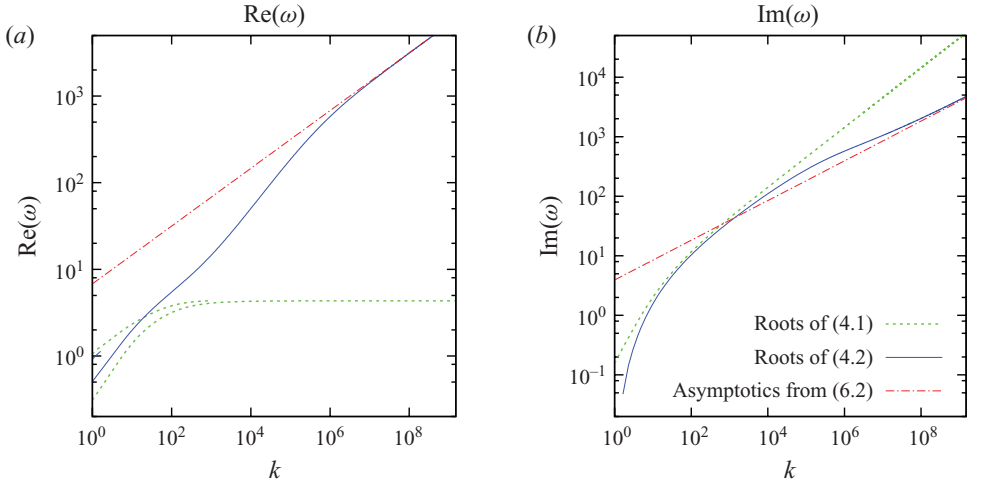


FIGURE 9. (Colour online) Trajectories of $\omega(k)$ as k is varied for the unbounded growth rate mode, plotted on a log–log scale, for the same situation as figure 8.

to leading order. Assuming a mass–spring–damping boundary so that $Z = \mathrm{i}a\omega + O(1)$ gives the leading-order solution to (6.1) for large real k of

$$\omega = \frac{\mathrm{e}^{-\mathrm{i}\pi/6} M^2 k^{1/3}}{0.777a\sqrt{1-M^2}((\gamma-1)u_y(0)T(0))^{2/3}}. \tag{6.3}$$

Since in this case $\omega = O(k^{1/3})$, our assumption of a caustic at the wall is self-consistent. The accuracy of this prediction is shown in figure 9. This figure also demonstrates the difference in behaviour seen by accounting for the boundary layer, since the unbounded growth rate for a mass–spring–damping boundary changes from $-\mathrm{Im}(\omega(k)) = O(k^{1/2})$ using the Myers boundary condition (4.4) to $-\mathrm{Im}(\omega(k)) = O(k^{1/3})$ when accounting for the boundary layer (4.5).

https://doi.org/10.1017/jfm.2011.116 Published online by Cambridge University Press

Since $\mathrm{Im}(\omega(k))$ is unbounded below for (4.5), it is expected that the viscous-boundary-layer model presented here will lead to the same numerical stability problems when simulated numerically in the time domain that the Myers boundary condition (4.4) suffers from. It is suggested here that, because of this similarity, it may be possible to regularize (4.5) and remove this unwanted unbounded growth rate in a similar way to the regularization of the Myers boundary condition (4.4) (see, e.g. Brambley 2011). However, the different asymptotic behaviour seen here may imply that such a regularization may not be as straightforward in the viscous case.

7. Conclusion

In this paper, we have given a thorough analysis of the response of a thin parallel boundary layer over a non-rigid boundary to small perturbations. The small perturbations may be acoustic but may also be small perturbations to an incompressible fluid. The governing equations (2.5) and boundary conditions (2.7) were derived under the assumption that the boundary layer was thin and parallel and the acoustic perturbations were small. The analysis presented here is valid for any boundary-layer profile, provided it is parallel and in thermal equilibrium with the boundary, so that $T_y(0)=0$. In particular, no assumption has been made restricting the change in velocity or temperature across the boundary layer to be small, as was assumed by Aurégan *et al.* (2001).

The distinction shown here between a compliant and a permeable boundary (sketched in figure 3) is notable in that this distinction appears not to have been made before, at least in this context. This may be because there is no distinction between these two types of boundaries either with inviscid fluid (as considered by, e.g. Eversman & Beckemeyer 1972; Tester 1973), since in this case there is no no-slip boundary condition, or for viscous flow over a fixed surface, since a fixed surface could be considered as either a permeable or a compliant boundary with an infinite impedance. Nayfeh (1973, equations (13) and (14)) explicitly considers only permeable boundaries, while for Aurégan *et al.* (2001, following equation (18)) the permeability assumption is stated as a fact.

As a summary of the behaviour discovered here, at high frequency or, equivalently, for well-developed boundary layers with $x_0 \gg 1$, the Myers boundary condition of the continuity of displacement across the boundary layer seems appropriate, as predicted by Aurégan *et al.* (2001). At low frequency we find the continuity of mass flux (as predicted by Aurégan *et al.* 2001) to be valid only for a permeable boundary, while a compliant boundary leads to a pressure-release boundary condition to leading order (which may be interpreted as compliance providing a yielding boundary, with the degree of compliance given in higher-order terms coming from the $O(1)$ terms in equation (5.5)). For large real k and a mass–spring–damper boundary, we find $\omega \sim A_1 \mathrm{e}^{-\mathrm{i}\pi/6}k^{1/3}$ for some positive constant A_1; this contrasts with the Myers boundary condition, which predicts $\omega \sim A_2 \mathrm{e}^{-\mathrm{i}\pi/2}k^{1/2}$ for some positive constant A_2. Since $\mathrm{Im}(\omega(k))$ is unbounded below, this model is predicted to suffer the same numerical instability when simulated numerically in the time domain, and possesses the same lack of a mathematical stability analysis, that the Myers boundary condition suffers from, although this could presumably be corrected in the same manner as for the Myers boundary condition (see Brambley 2011, for details).

In the high-frequency limit, there is a branch cut when $\mathrm{i}(\omega - Mk)$ is both real and negative, and for a permeable boundary there exists an anomalous region of the k-plane (bounded by this branch cut and a caustic) within which the continuity of

https://doi.org/10.1017/jfm.2011.116 Published online by Cambridge University Press

displacement appears not to hold. This region was unseen by Aurégan *et al.* since they considered the limit in which the mean-flow temperature and velocity varied little across the boundary layer, putting the branch cut and any anomalous region at infinity. It is unclear whether this region is an artefact of the approximations used here or whether it has some physical significance.

While the validity of any of these assumptions made here may be questioned in any particular scenario, what has unquestionably been shown here is that the permeable or compliant nature of the boundary together with the inclusion of dissipative terms within the boundary layer (such as viscosity and thermal conductivity) can lead to dramatically different behaviour than would be seen if they had been ignored. For example, figure 4 and § 5.3 show the dramatic difference between a compliant boundary (figure 4*a,b*) and a permeable boundary (figure 4*c,d*) at high frequency; §§ 4.2, 5.1 and 5.2 show that for low frequencies the Myers boundary condition is not appropriate, and that dissipative terms cause different leading-order effects for compliant and permeable boundaries; figure 6 shows three new modes in the anomalous region due to dissipation in an aeroacoustically relevant parameter range and figure 9 shows asymptotically different surface-mode behaviour when dissipation is included compared with the Myers boundary condition.

The author would like to thank Professor N. Peake for his encouragement and guidance. This work was supported by a Research Fellowship from Gonville & Caius College, Cambridge, UK.

Appendix A. Frobenius expansion about a critical layer

We investigate the behaviour of the linearized governing equations (2.5) about a point y_0 at which $\omega - u(y_0)k = 0$. The point y_0 is referred to as a *critical layer* (Vilenski & Rienstra 2007, and references therein). Setting $z = y - y_0$, we pose the Frobenius expansion (see, e.g. Riley, Hobson & Bence 2002, § 16.3) for small z:

$$\tilde{v} = z^{\nu}\sum_{n=0}^{\infty}\tilde{v}_n z^n, \quad \tilde{u} = z^{\mu}\sum_{n=0}^{\infty}\tilde{u}_n z^n, \quad \tilde{T} = z^{\tau}\sum_{n=0}^{\infty}\tilde{T}_n z^n, \tag{A 1a}$$

$$u = \sum_{n=0}^{\infty}u_n z^n, \quad T = \sum_{n=0}^{\infty}T_n z^n, \tag{A 1b}$$

with none of the leading coefficients being zero. (Note that, in this section, $\tilde{v}_0$ is the leading coefficient in the expansion of $\tilde{v}$ and not the normal velocity at the wall as elsewhere in the paper.) Looking at only the terms that could potentially be leading-order, the leading-order terms of (2.5) will be the leading-order terms of

$$-\mathrm{i}u_1 k\tilde{T}_0 z^{\tau+1} - T_0\nu\tilde{v}_0 z^{\nu-1} + (T_1\tilde{v}_0 - T_0\tilde{v}_1)z^{\nu} + \mathrm{i}kT_0\tilde{u}_0 z^{\mu} = 0; \tag{A 2a}$$

$$\begin{aligned}-\frac{u_1\tilde{v}_0 z^{\nu}}{(\gamma-1)^2 T_0} &+ \mu(\mu-1)T_0\tilde{u}_0 z^{\mu-2} + \mu[(\mu+1)T_0\tilde{u}_1 \\ &+ T_1\tilde{u}_0]z^{\mu-1} + (\mu+1)[(\mu+2)T_0\tilde{u}_2 + T_1\tilde{u}_1]z^{\mu} + \tau u_1\tilde{T}_0 z^{\tau-1} \\ &+ [(\tau+1)u_1\tilde{T}_1 + 2u_2\tilde{T}_0]z^{\tau} = 0;\end{aligned} \tag{A 2b}$$

$$\begin{aligned}-\frac{T_1\tilde{v}_0 z^{\nu}}{(\gamma-1)^2 T_0} &+ \frac{1}{Pr}[\tau(\tau-1)T_0\tilde{T}_0 z^{\tau-2} + \tau[(\tau+1)T_0\tilde{T}_1 + 2T_1\tilde{T}_0]z^{\tau-1} \\ &+ [(\tau+2)(\tau+1)T_0\tilde{T}_2 + 2(\tau+1)T_1\tilde{T}_1 + 2T_2\tilde{T}_0 + Pr(u_1)^2\tilde{T}_0]z^{\tau}] \\ &+ 2T_0u_1\tilde{u}_0\mu z^{\mu-1} + 2T_0u_1\tilde{u}_1(\mu+1)z^{\mu} = 0.\end{aligned} \tag{A 2c}$$

https://doi.org/10.1017/jfm.2011.116 Published online by Cambridge University Press

Specify	ν	μ	τ	Extra conditions
$\tilde{v}_0 = \tilde{v}(y_0)$	0	2	2	
$\tilde{u}_0 = \tilde{u}'(y_0)$	2	1	2	
$\tilde{T}_0 = \tilde{T}'(y_0)$	3	2	1	
$\tilde{u}_0 = \tilde{u}(y_0)$	1	0	3	$\tilde{u}_1 = 1$
$\tilde{T}_0 = \tilde{T}(y_0)$	2	2	0	$\tilde{T}_1 = 0$

TABLE 2. Leading-order coefficients for a Frobenius expansion about a critical layer.

We now look for values of (ν, μ, τ) that allow these three equations to be satisfied. If $\nu \neq 0$ and $\mu \notin \{0, 1\}$ and $\tau \notin \{0, 1\}$, then we would need to balance two terms in each equation with powers of z:

$$\left.\begin{array}{llll} (a) & \nu - 1 & \mu & \tau + 1 \\ (b) & \nu & \mu - 2 & \tau - 1 \\ (c) & \nu & \mu - 1 & \tau - 2 \end{array}\right\} \tag{A 3}$$

By considering the three possible pairings of terms in (c), we find that no solutions of this form exist. Therefore, either $\nu = 0$ or $\mu \in \{0, 1\}$ or $\tau \in \{0, 1\}$. Considering $\nu = 0$, we find that (A 2b) and (A 2c) imply that $\mu = \tau = 2$ (we cannot have $\mu, \tau \in \{0, 1\}$ as this would give an underdetermined system of equations for the coefficients), and that in this case (A 2a) then gives an equation for $\tilde{v}_1$ in terms of $\tilde{v}_0$. Hence, we may take $(\nu, \mu, \tau) = (0, 2, 2)$ and specify $\tilde{v}_0$, with all other coefficients then being uniquely determined. Proceeding like this, five solutions are given in table 2, which can easily be seen to be independent. The reason for the extra conditions is that, without these, the fourth and fifth solutions would contain an arbitrary multiple of the second and third solutions. Since the set of equations are fifth order in total, these are all the solutions. Since all the exponents are non-negative, the governing equations (2.5) are regular even at $y = y_0$, unlike the linearized Euler equations for shear flows, showing that viscosity regularizes the critical layer.

Appendix B. Low-frequency asymptotics for permeable boundaries

In this section we derive the low-frequency asymptotics for $\tilde{v}_\infty/\tilde{v}_0$ for a permeable boundary. Rewriting the governing equations (2.5) gives

$$\left(\frac{\tilde{v}}{T}\right)_y = \frac{\mathrm{i}\omega}{T^2}\left[\left(1 - \frac{uk}{\omega}\right)\tilde{T} + \frac{k}{\omega}T\tilde{u}\right], \tag{B 1a}$$

$$(T\tilde{u}_y + \tilde{T}u_y)_y - \frac{u_y\tilde{v}}{(\gamma-1)^2T} = \frac{\mathrm{i}\omega}{(\gamma-1)^2T}\left(1 - \frac{uk}{\omega}\right)\tilde{u}, \tag{B 1b}$$

$$\frac{1}{Pr}(\tilde{T}T)_{yy} + \tilde{T}(u_y)^2 + 2Tu_y\tilde{u}_y - \frac{T_y\tilde{v}}{(\gamma-1)^2T} = \frac{\mathrm{i}\omega}{(\gamma-1)^2T}\left(1 - \frac{uk}{\omega}\right)\tilde{T}. \tag{B 1c}$$

Setting $\bar{\eta}_\infty^2 = \mathrm{i}(1 - Mk/\omega)$ with $\mathrm{Re}\,\bar{\eta}_\infty > 0$, expanding the exact result for $y > Y$ from (3.2) in powers of ω gives

$$\tilde{v} = \tilde{v}_\infty - \omega^{1/2}\left[\frac{\bar{\eta}_\infty}{\sigma}(\gamma-1)\tilde{T}_\infty + \frac{\mathrm{i}k}{\omega\bar{\eta}_\infty}\tilde{u}_\infty\right] + \omega y\left[(\gamma-1)\bar{\eta}_\infty^2\tilde{T}_\infty + \frac{\mathrm{i}k}{\omega}\tilde{u}_\infty\right] + O(\omega^{3/2}), \tag{B 2a}$$

$$\tilde{u} = \tilde{u}_\infty - \omega^{1/2}\bar{\eta}_\infty y\tilde{u}_\infty + \tfrac{1}{2}\omega\bar{\eta}_\infty^2 y^2\tilde{u}_\infty + O(\omega^{3/2}), \tag{B 2b}$$

$$\tilde{T} = \tilde{T}_\infty - \omega^{1/2}\sigma\bar{\eta}_\infty y\tilde{T}_\infty + \tfrac{1}{2}\omega\sigma^2\bar{\eta}_\infty^2 y^2\tilde{T}_\infty + O(\omega^{3/2}). \tag{B 2c}$$

https://doi.org/10.1017/jfm.2011.116 Published online by Cambridge University Press

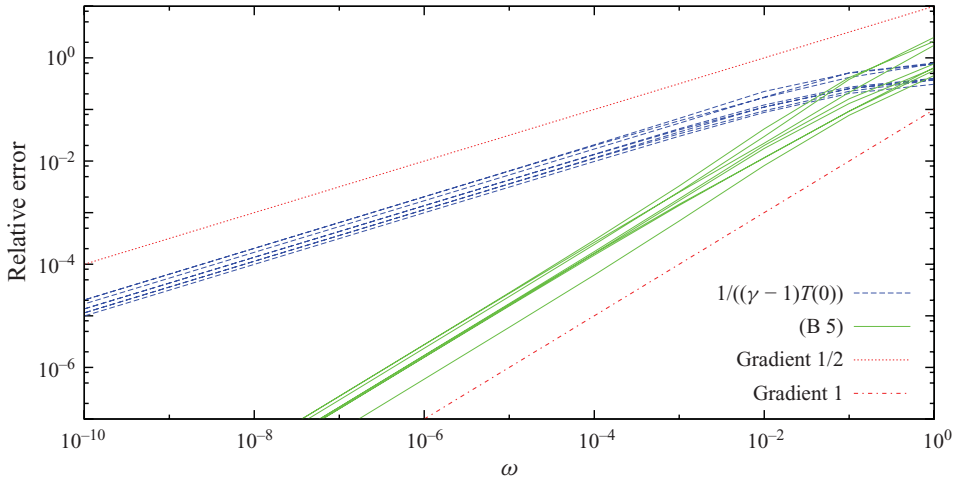


FIGURE 10. (Colour online) Log–log plot of the relative error of (B 6). (If a quantity $q = Q + \delta q$, where Q is the correct value and δq is the absolute error, then the relative error is $\delta q/Q$.) The solid lines show the variation of the error as ω is varied with the other parameters fixed. The long-dashed lines are the same for just the leading-order term. The dotted and dash-dotted lines have slope 1/2 and 1 respectively. Parameters are $k/\omega = \pm 1, \pm\mathrm{i}, \pm 1 \pm \mathrm{i}, \pm 1 \mp \mathrm{i}$, with $M = 0.5$, $Pr = 0.7$, $\gamma = 1.4$ and $x_0 = 1$.

We will match the inner solution to this expansion.

For the inner expansion, we expand in powers of $\omega^{1/2}$, so that $\tilde{v} = \tilde{v}_0 + \omega^{1/2}\tilde{v}_1 + \cdots$. Then (B 1$a$), to leading order, gives $\tilde{v}_0 = T/T(0)$, which is the continuity of mass flux across the boundary layer. At leading order, (B 1b) may be integrated once, and matching with the outer solution sets the constant of integration, to give

$$T\tilde{u}_{0y} + \tilde{T}_0 u_y = \frac{u - M}{(\gamma - 1)^2 T(0)}. \tag{B 3}$$

Taking the leading-order part of (B 1c) and subtracting $2u_y$ times (B 3) leads to the leading-order equation for $\tilde{T}_0$:

$$\frac{1}{Pr}(T\tilde{T}_0)_{yy} - \tilde{T}_0 (u_y)^2 = \frac{T_y + 2u_y(M - u)}{(\gamma - 1)^2 T(0)}. \tag{B 4}$$

The boundary conditions to apply to these are that $\tilde{u}_0(0) = \tilde{T}_0(0) = 0$ and that $\tilde{T}_0$ tends to a constant as $y \to \infty$. Solving (B 4) for $\tilde{T}_0$ gives $\tilde{T}_\infty = \tilde{T}_0(\infty) + O(\omega^{1/2})$. Then (B 3) gives

$$\tilde{u}_0 = \int_0^y \frac{u - M}{(\gamma - 1)^2 T(0) T} - \frac{\tilde{T}_0 u_y}{T}\,\mathrm{d}y', \tag{B 5}$$

and $\tilde{u}_\infty = \tilde{u}_0(\infty) + O(\omega^{1/2})$. Finally, this gives

$$\tilde{v}_\infty = \frac{1}{(\gamma - 1)T(0)} + \omega^{1/2}\left[\frac{\bar{\eta}_\infty}{\sigma}(\gamma - 1)\tilde{T}_\infty + \frac{\mathrm{i}k}{\omega\bar{\eta}_\infty}\tilde{u}_\infty\right] + O(\omega). \tag{B 6}$$

This gives the first two terms of the asymptotic expansion for $\tilde{v}_\infty/\tilde{v}_0$ in the low-frequency limit for a permeable boundary. Setting $\tilde{T}_0(y) = F(y)$ and $\tilde{u}_\infty = A$ in (B 6) gives the expression given in (5.2).

These asymptotic results have been verified against numerical results for numerous values of all parameters. Figure 10 shows an example of this verification, plotting the

https://doi.org/10.1017/jfm.2011.116 Published online by Cambridge University Press

relative error in $\tilde{v}_\infty$ for a few parameter values, and clearly showing that the error in (B 6) is $O(\omega)$.

Appendix C. Low-frequency asymptotics for compliant boundaries

In this section we derive the low-frequency asymptotics for $\tilde{v}_\infty/\tilde{v}_0$ for a compliant boundary. The $\tilde{u}$ boundary condition in (2.7) implies $\tilde{u} = O(1/\omega)$, so we set $\tilde{u} = \mathrm{i}u_y(0)/\omega + \bar{u}$, giving the governing equations

$$\left(\frac{\tilde{v}}{T}\right)_y + \frac{u_y(0)k}{T\omega} = \frac{\mathrm{i}\omega}{T^2}\left[\left(1 - \frac{uk}{\omega}\right)\tilde{T} + \frac{k}{\omega}T\bar{u}\right], \quad (\mathrm{C}\,1a)$$

$$(T\bar{u}_y + \tilde{T}u_y)_y - \frac{u_y\tilde{v}}{(\gamma-1)^2T} + \left(1 - \frac{uk}{\omega}\right)\frac{u_y(0)}{(\gamma-1)^2T} = \frac{\mathrm{i}\omega}{(\gamma-1)^2T}\left(1 - \frac{uk}{\omega}\right)\bar{u}, \quad (\mathrm{C}\,1b)$$

$$\frac{1}{Pr}(\tilde{T}T)_{yy} + \tilde{T}(u_y)^2 + 2Tu_y\bar{u}_y - \frac{T_y\tilde{v}}{(\gamma-1)^2T} = \frac{\mathrm{i}\omega}{(\gamma-1)^2T}\left(1 - \frac{uk}{\omega}\right)\tilde{T}, \quad (\mathrm{C}\,1c)$$

with boundary conditions $\bar{u}(0) = \tilde{T}(0) = 0$, $\tilde{v}(0) = 1$. Matching with the outer solution (B 2*b*) gives $\tilde{u}_\infty = \mathrm{i}u_y(0)/\omega$ to leading order and implies that $\bar{u} = O(\omega^{-1/2})$. Since $\tilde{T}$ is forced by $\bar{u}$, this implies $\tilde{T} = O(\omega^{-1/2})$, while the boundary condition at $y = 0$ and (C 1*a*) together imply that $\tilde{v} = O(1)$. We therefore expand

$$\bar{u} = \bar{u}_{-1}\omega^{-1/2} + \bar{u}_0 + \cdots, \quad \tilde{T} = \tilde{T}_{-1}\omega^{-1/2} + \tilde{T}_0 + \cdots, \quad \tilde{v} = \tilde{v}_0 + \tilde{v}_1\omega^{1/2} + \cdots. \quad (\mathrm{C}\,2)$$

To leading order, (C 1) become

$$\left(\frac{\tilde{v}_0}{T}\right)_y + \frac{u_y(0)k}{T\omega} = 0, \quad (\mathrm{C}\,3a)$$

$$(T\bar{u}_{-1y} + \tilde{T}_{-1}u_y)_y = 0, \quad (\mathrm{C}\,3b)$$

$$\frac{1}{Pr}(\tilde{T}_{-1}T)_{yy} + \tilde{T}_{-1}(u_y)^2 + 2Tu_y\bar{u}_{-1y} = 0, \quad (\mathrm{C}\,3c)$$

with boundary conditions $\bar{u}_{-1}(0) = \tilde{T}_{-1}(0) = 0$, $\tilde{v}_0(0) = 1$, $\tilde{T}_{-1y}(\infty) = 0$ and $\bar{u}_{-1y}(\infty) = -\mathrm{i}\bar{\eta}_\infty u_y(0)$. Hence,

$$T\bar{u}_{-1y} + \tilde{T}_{-1}u_y = -\mathrm{i}\bar{\eta}_\infty u_y(0)/(\gamma-1), \quad (\mathrm{C}\,4a)$$

$$\frac{1}{Pr}(\tilde{T}_{-1}T)_{yy} - \tilde{T}_{-1}(u_y)^2 = 2\mathrm{i}\bar{\eta}_\infty u_y(0)/(\gamma-1)u_y. \quad (\mathrm{C}\,4b)$$

Let $f(y)$ be the solution of

$$\frac{1}{Pr}(Tf)_{yy} - (u_y)^2 f = -2u_y, \quad (\mathrm{C}\,5)$$

subject to $f(0) = f_y(\infty) = 0$. Then

$$\tilde{T}_{-1} = -\mathrm{i}\bar{\eta}_\infty u_y(0)f/(\gamma-1), \quad \bar{u}_{-1} = -\mathrm{i}\bar{\eta}_\infty u_y(0)\int_0^y \frac{1 - u_y f}{(\gamma-1)T}\,\mathrm{d}y, \quad (\mathrm{C}\,6a)$$

$$\tilde{v}_0 = \frac{T}{T(0)} - \frac{k}{\omega}u_y(0)(\gamma-1)T\int_0^y \frac{1}{(\gamma-1)T}\,\mathrm{d}y. \quad (\mathrm{C}\,6b)$$

https://doi.org/10.1017/jfm.2011.116 Published online by Cambridge University Press

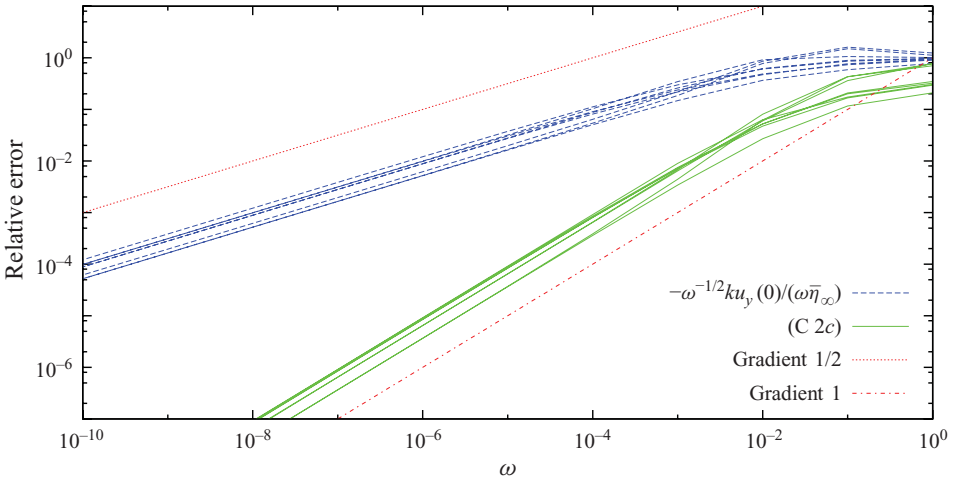


FIGURE 11. (Colour online) Log–log plot of the relative error of (5.5), similar to figure 10. The long-dashed lines are for just the leading-order term of (5.5), while the solid lines include all terms.

This matches the solution at infinity (B 2), provided

$$\tilde{T}_\infty = -\omega^{-1/2}\frac{\mathrm{i}\bar{\eta}_\infty u_y(0)}{(\gamma-1)}f(\infty) \qquad + O(1), \tag{C 7a}$$

$$\tilde{u}_\infty = \frac{\mathrm{i}u_y(0)}{\omega} + \mathrm{i}\bar{\eta}_\infty u_y(0)\omega^{-1/2}\int_0^\infty 1 - \frac{1-u_y f}{(\gamma-1)T}\,\mathrm{d}y \qquad + O(1), \tag{C 7b}$$

$$\begin{aligned}\tilde{v}_\infty = {} & -\omega^{-1/2}\frac{ku_y(0)}{\omega\bar{\eta}_\infty} + (1-Mk/\omega)\frac{u_y(0)f(\infty)}{\sigma} \\ & - \frac{ku_y(0)}{\omega}\int_0^\infty \frac{u_y f}{(\gamma-1)T}\,\mathrm{d}y + \frac{1}{(\gamma-1)T(0)} \qquad + O(\sqrt{\omega}).\end{aligned} \tag{C 7c}$$

This is the expression given in (5.5).

Figure 11 shows the log–log plot of the relative error against ω comparable to figure 10 and verifies that the asymptotics above are correct to the stated order.

Appendix D. High-frequency/short-wavelength asymptotics

In this appendix, we solve the governing equations (2.5) in the high-frequency limit $\omega \gg 1$ with $k/\omega \leqslant O(1)$, and in the short-wavelength limit $k \gg 1$ with $\omega/k \leqslant O(1)$, using the method of multiple scales (see, e.g. Hinch 1991). To cover these two cases together, we define

$$\omega \gg 1, \qquad k \gg 1, \tag{D 1a}$$

$$\varepsilon = \omega^{-1/2}, \qquad \varepsilon = k^{-1/2}, \tag{D 1b}$$

$$L = k/\omega, \qquad L = 1, \tag{D 1c}$$

$$\bar{\eta}^2 = \frac{\mathrm{i}(1-uk/\omega)}{(\gamma-1)^2T^2}, \qquad \bar{\eta}^2 = \frac{-\mathrm{i}(u-\omega/k)}{(\gamma-1)^2T^2}. \tag{D 1d}$$

https://doi.org/10.1017/jfm.2011.116 Published online by Cambridge University Press

In either case, $\bar{\eta}$ is taken such that $\mathrm{Re}(\bar{\eta}(y)/\varepsilon) > 0$ as $y \to \infty$ and $\bar{\eta}(y)$ is a smooth function of y. We pose the multiple-scale WKB ansatz

$$\frac{\mathrm{d}}{\mathrm{d}y} = \frac{\partial}{\partial \hat{y}} + \frac{1}{\varepsilon}\bar{\eta}(\hat{y})\frac{\partial}{\partial \theta}. \tag{D 2}$$

This yields the same system of equations when evaluated along

$$\hat{y}(y) = y, \quad \theta(y) = \frac{1}{\varepsilon}\int_0^y \bar{\eta}(y')\,\mathrm{d}y'. \tag{D 3}$$

To avoid cluttering the notation, we now write $\hat{y}$ as y without ambiguity. In order to balance the terms, we find that $\tilde{v} = O(1/\varepsilon)$, and so we introduce $\tilde{v} = \tilde{\tilde{v}}/\varepsilon$. Substituting this into (2.5) gives the system of equations

$$\bar{\eta}^2(\gamma-1)^2 T\tilde{T} - \bar{\eta}\tilde{\tilde{v}}_\theta + \mathrm{i}L\tilde{u} = \varepsilon T\left(\frac{\tilde{\tilde{v}}}{T}\right)_y, \tag{D 4a}$$

$$\tilde{u}_{\theta\theta} - \tilde{u} = \frac{\varepsilon\tilde{\tilde{v}}u_y}{(\gamma-1)^2T^2\bar{\eta}^2} - \frac{\varepsilon}{T\bar{\eta}^2}[T_y\bar{\eta}\tilde{u}_\theta + 2T\bar{\eta}\tilde{u}_{\theta y} + T\bar{\eta}_y\tilde{u}_\theta + \bar{\eta}u_y\tilde{T}_\theta] - \frac{\varepsilon^2}{T\bar{\eta}^2}(T\tilde{u}_y + \tilde{T}u_y)_y, \tag{D 4b}$$

$$\frac{1}{Pr}\tilde{T}_{\theta\theta} - \tilde{T} = \frac{\varepsilon\tilde{\tilde{v}}T_y}{(\gamma-1)^2T^2\bar{\eta}^2} - \frac{\varepsilon}{PrT\bar{\eta}^2}[2\bar{\eta}(T\tilde{T}_\theta)_y + \bar{\eta}_yT\tilde{T}_\theta + 2PrTu_y\bar{\eta}\tilde{u}_\theta] - \frac{\varepsilon^2}{T\bar{\eta}^2}\left[\frac{1}{Pr}(T\tilde{T})_{yy} + \tilde{T}(u_y)^2 + 2Tu_y\tilde{u}_y\right]. \tag{D 4c}$$

We now solve this using the series $\tilde{u} = \tilde{u}_0 + \varepsilon\tilde{u}_1 + \cdots$ on the assumption that $\bar{\eta}(y) \neq 0$ for any y (this assumption will be relaxed in § D.1).

At $O(1)$, setting $\sigma = +\sqrt{Pr}$ and appealing to the boundary condition of decay at infinity of $\tilde{u}$ and $\tilde{T}$, we get

$$\tilde{u}_0 = B_0\,\mathrm{e}^{-\theta}, \quad \tilde{T}_0 = D_0\,\mathrm{e}^{-\sigma\theta}, \quad \tilde{\tilde{v}}_0 = E_0 - \mathrm{i}LB_0/\bar{\eta}\,\mathrm{e}^{-\theta} - \bar{\eta}(\gamma-1)^2TD_0/\sigma\,\mathrm{e}^{-\sigma\theta}. \tag{D 5}$$

At $O(\varepsilon)$, we prevent a secular term proportional to $\mathrm{e}^{-\theta}$ arising in (D 4*b*). While it is perhaps confusing to describe this term as secular, since the exponentials are exponentially increasing and decreasing, the term *secular* may be justified by taking y to be complex along a path such that $\mathrm{Re}(\theta)$ is constant; as will be seen when the asymptotics are compared to numerical solutions, the results derived using this method are valid. Preventing such a secular term in (D 4*b*) gives

$$(T^3\bar{\eta}^3{B_0}^2)_y = 0, \tag{D 6}$$

and solving for $\tilde{u}_1$ gives

$$\tilde{u}_1 = B_1\,\mathrm{e}^{-\theta} - \frac{E_0u_y}{(\gamma-1)^2T^2\bar{\eta}^2} + \frac{u_y}{\sigma\bar{\eta}T}D_0\,\mathrm{e}^{-\sigma\theta}. \tag{D 7}$$

Similarly, preventing a secular term proportional to $\mathrm{e}^{-\sigma\theta}$ arising in (D 4) gives

$$\left(\bar{\eta}T{D_0}^2\right)_y = 0, \tag{D 8}$$

and solving for $\tilde{T}_1$ (assuming $Pr \neq 1$) gives

$$\tilde{T}_1 = D_1\,\mathrm{e}^{-\sigma\theta} - \frac{E_0T_y}{(\gamma-1)^2T^2\bar{\eta}^2} - \frac{Pr}{(1-Pr)\bar{\eta}}\left(\frac{\mathrm{i}LT_y}{(\gamma-1)^2T^2\bar{\eta}^2} - 2u_y\right)B_0\,\mathrm{e}^{-\theta}. \tag{D 9}$$

https://doi.org/10.1017/jfm.2011.116 Published online by Cambridge University Press

Finally, preventing a secular term arising in (D 4*a*) gives

$$\left(\frac{E_0}{(\gamma-1)^2T^2\bar{\eta}^2}\right)_y = 0 \tag{D 10}$$

which is the continuity of displacement, agreeing with the prediction of Aurégan *et al.* (2001). Solving for $\tilde{\tilde{v}}_1$ gives

$$\begin{aligned}\tilde{\tilde{v}}_1 = E_1 - \frac{\mathrm{i}L}{\bar{\eta}}B_1\,\mathrm{e}^{-\theta} - \frac{(\gamma-1)^2\bar{\eta}T}{\sigma}D_1\,\mathrm{e}^{-\sigma\theta} - \frac{(\gamma-1)^2\bar{\eta}T^3}{Pr}\left(\frac{D_0}{\bar{\eta}T^2}\right)_y\mathrm{e}^{-\sigma\theta}\\ + \left[\frac{1}{(1-Pr)\bar{\eta}T}(\mathrm{i}LT_y - 2Pru_y(\gamma-1)^2T^2\bar{\eta}^2) - \frac{\mathrm{i}L}{\bar{\eta}}\frac{\partial}{\partial y}\right](B_0/\eta)\,\mathrm{e}^{-\theta}.\end{aligned} \tag{D 11}$$

We may now apply the boundary conditions at $y=0$ to the leading-order solution, to find that $B_0 = D_0 = 0$ and that $E_0 = (T^2\bar{\eta}^2)/(T(0)^2\bar{\eta}(0)^2) \equiv 1 - uk/\omega$.

At $O(\omega^{-1})$, exactly the same secularity conditions as above occur. However, this time the boundary conditions are $\tilde{u}_1(0) = \mathrm{i}Cku_y(0)/(\omega L)$ and $\tilde{\tilde{v}}_1(0) = \tilde{T}_1(0) = 0$, giving

$$B_1(0) = -(1-C)\frac{\mathrm{i}k}{L\omega}u_y(0), \quad E_1(0) = (1-C)\frac{ku_y(0)}{\omega\bar{\eta}(0)}, \quad D_1 \equiv 0. \tag{D 12}$$

Note that for a compliant boundary (with $C=1$), all of these terms are zero. In fact, for a compliant boundary, it can be shown that $\tilde{u}_2 = \tilde{T}_2 = 0$.

In summary, and in terms of $\tilde{v} = \tilde{\tilde{v}}/\varepsilon$, for a compliant boundary,

$$\left.\begin{aligned}&\tilde{v} = 1 - uk/\omega + O(\varepsilon^2), \quad \tilde{u} = \mathrm{i}u_y/\omega + O(\varepsilon^4), \quad \tilde{T} = \mathrm{i}T_y/\omega + O(\varepsilon^4),\\ &Z_{eff} = \frac{Z}{1-Mk/\omega} + O(\varepsilon^2),\end{aligned}\right\} \tag{D 13}$$

while for a permeable boundary,

$$\left.\begin{aligned}&\tilde{v} = \left(1-\frac{uk}{\omega}\right)\left[1+\varepsilon\frac{ku_y(0)}{\omega\bar{\eta}(0)}\right] - \varepsilon\frac{ku_y(0)}{\omega\bar{\eta}}\left(1-\frac{uk}{\omega}\right)^{-3/4}\mathrm{e}^{-\theta} + O(\varepsilon^2),\\ &\tilde{u} = \frac{\mathrm{i}u_y}{\omega} - \frac{\mathrm{i}u_y(0)}{\omega}\left(1-\frac{uk}{\omega}\right)^{-3/4}\mathrm{e}^{-\theta} + O(\varepsilon^3), \quad \tilde{T} = \frac{\mathrm{i}T_y}{\omega} + O(\varepsilon^3),\\ &Z_{eff} = \frac{Z}{1-Mk/\omega}\left[1-\frac{\varepsilon u_y(0)k}{\bar{\eta}(0)\omega}\right] + O(\varepsilon^2).\end{aligned}\right\} \tag{D 14}$$

These asymptotic results have been verified against numerical results for numerous values of all parameters. Figure 12 shows the relative error in the asymptotics for a few parameters, demonstrating the correctness of (D 13) and (D 14) to the stated order of accuracy.

D.1. *The caustic*

The derivation above assumes $\bar{\eta}(y) \neq 0$ for any y. We now suppose that there is a y_0 such that $\bar{\eta}(y_0) = 0$. This occurs when $\omega/k = u(y_0)$, which is exactly the critical layer for an inviscid boundary layer (Pridmore-Brown 1958; Vilenski & Rienstra 2007). In Appendix A we saw that viscosity regularizes this critical layer, and so y_0 is an ordinary point of the differential equations (2.5). However, (D 6) is clearly singular at y_0. In fact, y_0 forms a caustic in the asymptotics above, caused by the fast multiple-scale variable θ and the slow variable $\hat{y}$ varying equally fast as $y \to y_0$. The relevant

https://doi.org/10.1017/jfm.2011.116 Published online by Cambridge University Press

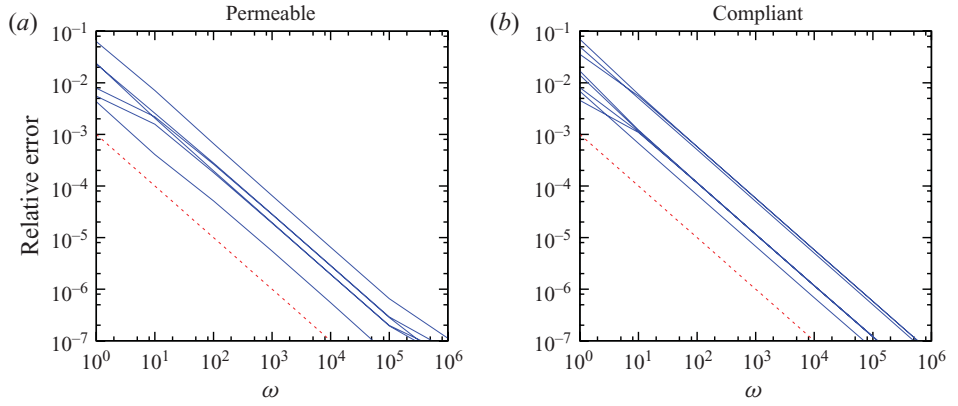


FIGURE 12. (Colour online) Log–log plot of the relative error of the high-frequency asymptotics for $\tilde{v}_\infty/\tilde{v}_0$, similar to figures 10 and 11. The dashed line has gradient -1.

rescaling turns out to be to consider $z = O(1)$, where

$$y = y_0 + \varepsilon^{2/3} Q^{1/3} z, \qquad Q = -\frac{(\gamma-1)^2 T(y_0)^2}{\mathrm{i} L u_y(y_0)}. \tag{D 15}$$

In what follows, branch cuts for all non-integer powers will be taken along the negative real axis, so that $\arg(z) = -\pi/6$ for $y > y_0$ and $\arg(z) = 5\pi/6$ for $y < y_0$. Based on this rescaling,

$$\bar{\eta}^2 = \varepsilon^{2/3} Q^{-2/3} z, \qquad \frac{\mathrm{d}}{\mathrm{d}y} = \varepsilon^{-2/3} Q^{-1/3} \frac{\mathrm{d}}{\mathrm{d}z}. \tag{D 16}$$

We now expand to leading order in ε about $y = y_0$ and match the resulting inner solution with the outer solution provided by the multiple-scale analysis of the previous section. Writing $\tilde{\tilde{v}} = \varepsilon^{-1/3}\tilde{\tilde{v}}$, (2.5) becomes

$$\mathrm{i} L T \tilde{u} - Q^{-1/3} T \tilde{\tilde{v}}_z = \varepsilon^{2/3}\left[\mathrm{i} L u_y Q^{1/3} z \tilde{T} - T_y \tilde{\tilde{v}}\right] + O(\varepsilon^{4/3}), \tag{D 17a}$$

$$\tilde{u}_{zz} - z\tilde{u} = \frac{\mathrm{i}\tilde{\tilde{v}}}{L Q^{1/3}} - \varepsilon^{2/3} \frac{u_y Q^{1/3}}{T} \tilde{T}_z + O(\varepsilon^{2/3}), \tag{D 17b}$$

$$\tilde{T}_{zz} - Prz\tilde{T} = \frac{\mathrm{i} Pr T_y \tilde{\tilde{v}}}{L u_y Q^{1/3}} - 2\varepsilon^{2/3} Pr u_y Q^{1/3} \tilde{u}_z + O(\varepsilon^{2/3}), \tag{D 17c}$$

where T, u_y and T_y are all evaluated at y_0. There are two possible scalings for $\tilde{T}$, but $\tilde{T} = O(\varepsilon^{-2/3})$ does not agree with our expectations from our outer solution, so we choose $\tilde{T} = O(1)$. This gives, to leading order,

$$\mathrm{i} L \tilde{u} - Q^{-1/3} \tilde{\tilde{v}}_z = 0, \tag{D 18a}$$

$$\tilde{u}_{zz} - z\tilde{u} = \frac{\mathrm{i}\tilde{\tilde{v}}}{L Q^{1/3}}, \tag{D 18b}$$

$$\tilde{T}_{zz} - Prz\tilde{T} = \frac{\mathrm{i} Pr T_y \tilde{\tilde{v}}}{L u_y Q^{1/3}}, \tag{D 18c}$$

and hence,

$$\tilde{u}_{zzz} - z\tilde{u}_z = 0, \qquad \tilde{\tilde{v}}_z = \mathrm{i} Q^{1/3} L \tilde{u}. \tag{D 19}$$

https://doi.org/10.1017/jfm.2011.116 Published online by Cambridge University Press

We may solve (D 19) using Fourier transforms, in a similar way to obtaining the asymptotics for Airy functions (see, e.g. Abramowitz & Stegun 1964), to get

$$\tilde{u}(z) = K_1 f_1(z) + K_2 f_1(z\,\mathrm{e}^{2\pi\mathrm{i}/3}) + K_3, \tag{D 20a}$$

$$\tilde{\tilde{v}}(z) = Q^{1/3} L[K_1 f_2(z) + K_2\,\mathrm{e}^{-2\pi\mathrm{i}/3} f_2(z\,\mathrm{e}^{2\pi\mathrm{i}/3}) + \mathrm{i}K_3 z], \tag{D 20b}$$

where

$$f_n = \frac{1}{2\pi}\int_{\mathscr{C}} \frac{1}{q^n}\exp\{\mathrm{i}(q^3/3 + qz)\}\,\mathrm{d}q, \tag{D 20c}$$

and the contour $\mathscr{C}$ is taken to be from $\infty\,\mathrm{e}^{5\mathrm{i}\pi/6}$ to $\infty\,\mathrm{e}^{\mathrm{i}\pi/6}$ and passing above any pole at $q=0$. Equation (D 20b) may then be used as a forcing term in (D 18c) to get the inner solution for $\tilde{T}$, but since this will not be used in what follows, we do not calculate that solution here. In order to match this with the outer solution, we need the large $|z|$ asymptotics of $f_n(z)$; these are derived later in § D.2. Using these asymptotics, for $y > y_0$,

$$\tilde{u}(z) \sim \frac{-\mathrm{i}K_1}{2\sqrt{\pi}z^{3/4}}\exp\left\{-\frac{2}{3}z^{3/2}\right\} - \frac{K_2}{2\sqrt{\pi}z^{3/4}}\exp\left\{\frac{2}{3}z^{3/2}\right\} + K_3, \tag{D 21a}$$

$$\tilde{\tilde{v}}(z) \sim \frac{-Q^{1/3}LK_1}{2\sqrt{\pi}z^{5/4}}\exp\left\{-\frac{2}{3}z^{3/2}\right\} - \frac{Q^{1/3}LK_2\,\mathrm{e}^{-5\pi\mathrm{i}/6}}{2\sqrt{\pi}z^{5/4}}\exp\left\{\frac{2}{3}z^{3/2}\right\} + \mathrm{i}Q^{1/3}LK_3 z. \tag{D 21b}$$

We now match this solution to the multiple-scale outer solution, which we take to be

$$\tilde{u} = (T\bar{\eta})^{-3/2}B_+\,\mathrm{e}^{-(\theta-\theta_0)} - \varepsilon E_+ u_y, \tag{D 22a}$$

$$\tilde{\tilde{v}} = E_+(\gamma-1)^2T^2\bar{\eta}^2 - \mathrm{i}LT^{-3/2}\bar{\eta}^{-5/2}B_+\,\mathrm{e}^{-(\theta-\theta_0)}, \tag{D 22b}$$

for $y > y_0$, where $\theta_0 = \theta(y_0)$. Noting that

$$\theta - \theta_0 = \frac{1}{\varepsilon}\int_{y_0}^{y}\bar{\eta}\,\mathrm{d}y = \frac{2}{3}z^{3/2} + O(\varepsilon^{2/3}), \tag{D 23}$$

expanding in terms of z to leading order,

$$\tilde{u} = T^{-3/2}\varepsilon^{-1/2}Q^{1/2}z^{-3/4}B_+\exp\left\{-\tfrac{2}{3}z^{3/2}\right\} - \varepsilon E_+ u_y, \tag{D 24a}$$

$$\tilde{\tilde{v}} = E_+(\gamma-1)^2T^2\varepsilon Q^{-2/3}z - \mathrm{i}LT^{-3/2}\varepsilon^{-1/2}Q^{5/6}z^{-5/4}B_+\exp\left\{-\tfrac{2}{3}z^{3/2}\right\}, \tag{D 24b}$$

so that (to the leading order considered here),

$$K_1 = 2\sqrt{\pi}\mathrm{i}T^{-3/2}\varepsilon^{-1/2}Q^{1/2}B_+, \quad K_2 = 0, \quad K_3 = -\varepsilon E_+ u_y. \tag{D 25}$$

Similarly, expanding the inner solution for $y < y_0$, so that $\arg(z) = 5\pi\mathrm{i}/6$, gives

$$\tilde{u} \sim \frac{Q^{1/2}B_+}{T^{3/2}\varepsilon^{1/2}z^{3/4}}\left[\exp\left\{-\frac{2}{3}z^{3/2}\right\} - \mathrm{i}\exp\left\{\frac{2}{3}z^{3/2}\right\}\right] + \frac{2\sqrt{\pi}Q^{1/2}B_+}{T^{3/2}\varepsilon^{1/2}} - \varepsilon E_+ u_y, \tag{D 26a}$$

$$\tilde{\tilde{v}} \sim \frac{-\mathrm{i}LQ^{5/6}B_+}{T^{3/2}\varepsilon^{1/2}z^{5/4}}\left[\exp\left\{-\frac{2}{3}z^{3/2}\right\} + \mathrm{i}\exp\left\{\frac{2}{3}z^{3/2}\right\}\right] + \frac{2\sqrt{\pi}\mathrm{i}LQ^{5/6}B_+}{T^{3/2}\varepsilon^{1/2}}z + E_+(\gamma-1)^2T^2\varepsilon Q^{-2/3}z. \tag{D 26b}$$

https://doi.org/10.1017/jfm.2011.116 Published online by Cambridge University Press

Taking the outer solution for $y < y_0$ to be

$$\tilde{u} = (T\bar{\eta})^{-3/2}[A_- \mathrm{e}^{\theta-\theta_0} + B_- \mathrm{e}^{-(\theta-\theta_0)}] - \varepsilon E_- u_y, \tag{D 27a}$$

$$\tilde{\tilde{v}} = E_-(\gamma-1)^2 T^2 \bar{\eta}^2 + \mathrm{i}LT^{-3/2}\bar{\eta}^{-5/2}[A_- \mathrm{e}^{\theta-\theta_0} - B_- \mathrm{e}^{-(\theta-\theta_0)}], \tag{D 27b}$$

in terms of z to leading order gives

$$\tilde{u} = T^{-3/2}\varepsilon^{-1/2}Q^{1/2}z^{-3/4}\left[A_- \exp\left\{\tfrac{2}{3}z^{3/2}\right\} + B_- \exp\left\{-\tfrac{2}{3}z^{3/2}\right\}\right], \tag{D 28a}$$

$$\tilde{\tilde{v}} = E_-(\gamma-1)^2 T^2 \varepsilon Q^{-2/3} z + \mathrm{i}LT^{-3/2}\varepsilon^{-1/2}Q^{5/6}z^{-5/4}\left[A_- \exp\left\{\tfrac{2}{3}z^{3/2}\right\} - B_- \exp\left\{-\tfrac{2}{3}z^{3/2}\right\}\right]. \tag{D 28b}$$

Hence,

$$A_- = -\mathrm{i}B_+, \quad B_- = B_+, \quad E_- = E_+ - \frac{2\sqrt{\pi}Q^{1/2}B_+}{T^{3/2}\varepsilon^{3/2}u_y}. \tag{D 29}$$

These conditions give the jump in coefficients across the caustic, to leading order.

In summary, if the solution for $y > y_0$ is

$$\tilde{u} = (T\bar{\eta})^{-3/2}B\,\mathrm{e}^{-\theta} - \varepsilon E_+ u_y, \tag{D 30a}$$

$$\tilde{\tilde{v}} = E_+(\gamma-1)^2T^2\bar{\eta}^2 - \mathrm{i}LT^{-3/2}\bar{\eta}^{-5/2}B\,\mathrm{e}^{-\theta}, \tag{D 30b}$$

then the solution for $y < y_0$, to leading order, is

$$\tilde{u} = (T\bar{\eta})^{-3/2}B[\mathrm{e}^{-\theta} - \mathrm{i}\exp\{\theta - 2\theta(y_0)\}] - \varepsilon E_- u_y, \tag{D 31a}$$

$$\tilde{\tilde{v}} = E_-(\gamma-1)^2T^2\bar{\eta}^2 - \mathrm{i}LT^{-3/2}\bar{\eta}^{-5/2}B[\mathrm{e}^{-\theta} + \mathrm{i}\exp\{\theta - 2\theta(y_0)\}], \tag{D 31b}$$

where

$$E_+ - E_- = \frac{2\sqrt{\pi}\,\mathrm{e}^{\mathrm{i}\pi/4}(\gamma-1)B\,\mathrm{e}^{-\theta(y_0)}}{L^{1/2}T(y_0)^{1/2}\varepsilon^{3/2}u_y(y_0)^{3/2}}. \tag{D 32}$$

We now consider some specific implications of this for $y_0 = O(1)$ and $y_0 = O(\varepsilon^{2/3})$.

D.1.1. *Caustic in the interior of the boundary layer*

For this case, we assume that y_0 lies sufficiently within the interior of the boundary layer that $y_0\varepsilon^{-2/3} \gg 1$. This in turn means that $\theta(y_0) \gg 1$, so that $\mathrm{e}^{-\theta(y_0)}$ and $\mathrm{e}^{\theta-2\theta(y_0)}$ are exponentially small for $y < y_0$. Hence, in this case, the asymptotic solution is exactly the same as if there had been no caustic. This has been confirmed by comparison with numerical results for sufficiently high frequencies.

D.1.2. *Caustic near the wall*

For this case, we assume that $y_0 = O(\varepsilon^{2/3})$ so that the boundary at $y = 0$ occurs within the inner scaling region of the caustic. This scaling implies that $\omega/k = \bar{\omega}\varepsilon^{2/3}$ with $\bar{\omega} = O(1)$, and that $k \gg 1$. We are therefore in the short-wavelength limit for which $\varepsilon = k^{-1/2}$ and $L = 1$. Setting $\omega - u(y_0)k = 0$ gives

$$y_0 = \frac{\bar{\omega}\varepsilon^{2/3}}{u_y(0)} + O(\varepsilon^{4/3}), \quad \theta_0 \equiv \theta(y_0) = -\frac{2}{3}\left(\frac{-\bar{\omega}}{u_y(0)Q^{1/3}}\right)^{3/2} + O(\varepsilon^{2/3}). \tag{D 33}$$

The solution for $y = O(1)$ is still given by (D 22*a*,*b*) and the solution within the caustic region by (D 20*a*,*b*), with K_1 and K_3 still given by matching the two (D 25). However, the boundary conditions $\tilde{\tilde{v}}(0) = \varepsilon^{4/3}$ and $\tilde{u}(0) = \mathrm{i}C\varepsilon^{4/3}u_y(0)/\bar{\omega}$ now fall within

https://doi.org/10.1017/jfm.2011.116 Published online by Cambridge University Press

the caustic region, and must be applied to the inner solution (D 20*a*,*b*). This leads to

$$\begin{pmatrix} C \\ 1 \end{pmatrix} = \begin{pmatrix} -A_{11} & 1 \\ A_{21} & 1 \end{pmatrix} \begin{pmatrix} B_+ T(0)^{-3/2} \varepsilon^{-11/6} \\ \mathrm{i} E_+ \bar{\omega} \varepsilon^{-1/3} \end{pmatrix} + O(\varepsilon^{2/3}), \tag{D 34}$$

where

$$A_{11} = -\frac{2\bar{\omega}}{u_y} \sqrt{\pi} Q^{1/2} f_1\left(\frac{-\bar{\omega}}{u_y Q^{1/3}}\right), \quad A_{21} = 2\sqrt{\pi}\mathrm{i} Q^{5/6} f_2\left(\frac{-\bar{\omega}}{u_y Q^{1/3}}\right), \tag{D 35}$$

and all functions of position (such as u_y) are evaluated at $y = 0$. Inverting gives

$$\frac{\tilde{v}_\infty}{\tilde{v}_0} = -\frac{Mk}{\omega} \frac{A_{11} + C A_{21}}{A_{11} + A_{21}} (1 + O(\varepsilon^{2/3})). \tag{D 36}$$

For a compliant boundary with $C = 1$, this is exactly what would have been obtained had the caustic been ignored. For a permeable boundary with $C = 0$, the caustic plays an important role, although in the limit $\bar{\omega} \to \infty$ the impact of the caustic disappears, as it has to recover the $y_0 = O(1)$ asymptotics above.

If $C = 0$ and $\bar{\omega}$ is small, expanding about $\bar{\omega} = 0$ gives

$$E_+ = \frac{\varepsilon^{1/3} f_1(0)}{Q^{1/3} u_y(0) f_2(0)} - \frac{\mathrm{i}\varepsilon^{1/3} \bar{\omega} f_0(0)}{u_y(0)^2 Q^{2/3} f_2(0)} + O(\bar{\omega}^2, \varepsilon), \tag{D 37a}$$

$$B_+ = \frac{-\mathrm{i}\varepsilon^{11/6} T(0)^{3/2}}{2\sqrt{\pi} Q^{5/6} f_2(0)} + O(\bar{\omega}^2, \varepsilon^{5/2}), \tag{D 37b}$$

which predicts, to leading order,

$$\frac{\tilde{v}_\infty}{\tilde{v}_0} = \frac{-\mathrm{e}^{\mathrm{i}\pi/3} k^{1/3} M f_1(0)}{u_y(0)^{2/3} f_2(0) (\gamma - 1)^{2/3} T(0)^{2/3}}. \tag{D 38}$$

Numerical calculation gives

$$f_0(0) \approx 0.355, \quad f_1(0) = -\mathrm{i}/3, \quad f_2(0) \approx -0.259, \tag{D 39}$$

so that $\arg(Z_{eff}/Z) = -1/3 \arg(-\mathrm{i}k)$ with $\arg(-\mathrm{i}k) \in (-\pi, \pi)$, while $|Z_{eff}/Z| = O(k^{-1/3})$ as $|k| \to \infty$.

D.2. *Asymptotics of* f_n

Here we derive the large $|z|$ asymptotics of

$$f_n(z) = \frac{1}{2\pi} \int_{\mathscr{C}} \frac{1}{q^n} \exp\{\mathrm{i}(q^3/3 + qz)\} \, \mathrm{d}q, \tag{D 40}$$

along a contour $\mathscr{C}$ from $\infty \mathrm{e}^{5\mathrm{i}\pi/6}$ to $\infty \mathrm{e}^{\mathrm{i}\pi/6}$ which passes above any pole at $q = 0$. We will do this using the method of steepest descent (see, for example, Hinch 1991), in a similar manner to the derivation of the asymptotics of the Airy function. Writing $z = r \mathrm{e}^{\mathrm{i}\theta}$, $q = r^{1/2}\tilde{q}$ and $\phi(\tilde{q}) = \mathrm{i}(\tilde{q}^3/3 + \tilde{q}\, \mathrm{e}^{\mathrm{i}\theta})$ gives

$$f_n(z) = \frac{1}{2\pi r^{(n-1)/2}} \int_{\mathscr{C}} \frac{1}{\tilde{q}^n} \exp\{r^{3/2}\phi(\tilde{q})\} \, \mathrm{d}\tilde{q}. \tag{D 41}$$

We now deform $\mathscr{C}$ onto a steepest descent contour, along which $\mathrm{Im}(\phi)$ is constant and $\mathrm{Re}(\phi)$ is bounded above. As an aid to locating this contour, we find the saddle points of ϕ to be at

$$\tilde{q}_m = \exp\{\mathrm{i}\theta/2 + \mathrm{i}\pi/2 - m\pi\}, \quad m \in \{0, 1\}, \tag{D 42}$$

https://doi.org/10.1017/jfm.2011.116 Published online by Cambridge University Press

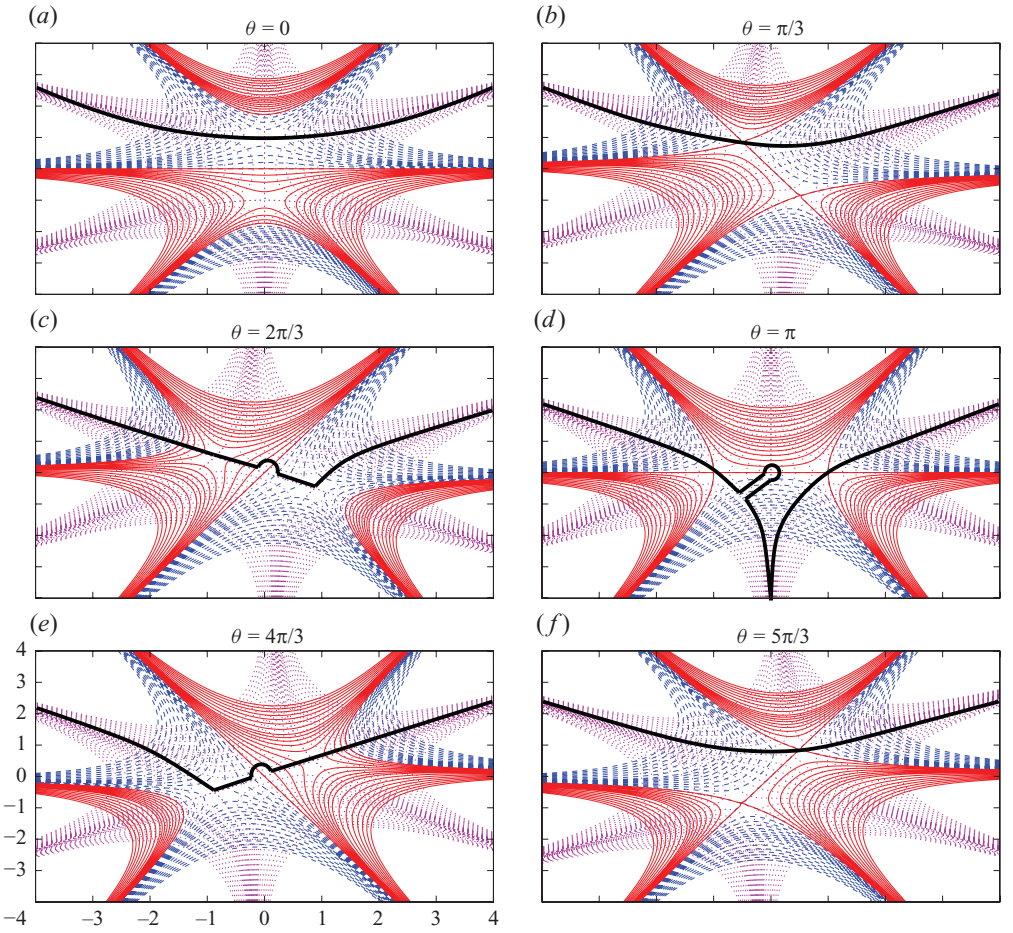


FIGURE 13. (Colour online) Contour plots of $\phi(\tilde{q}) = \mathrm{i}(\tilde{q}^3/3 + \tilde{q}\,\mathrm{e}^{\mathrm{i}\theta})$. The thin solid lines and dashed lines are the contours of $\mathrm{Re}(\phi)$ for $\mathrm{Re}(\phi) < 0$ and $\mathrm{Re}(\phi) > 0$ respectively. The dotted lines are the contours of $\mathrm{Im}(\phi)$. The thick solid line is the contour $\mathscr{C}$, traversed from left to right.

in the neighbourhood of which,

$$\phi(\tilde{q}) = -\tfrac{2}{3}\,\mathrm{e}\{3\mathrm{i}\theta/2 - m\pi\mathrm{i}\} - \mathrm{e}\{\mathrm{i}\theta/2 - m\pi\mathrm{i}\}(\tilde{q} - \tilde{q}_m)^2 + O((\tilde{q} - \tilde{q}_m)^3). \tag{D 43}$$

Locally about these saddle points, the steepest descent path, indexed by the real variable p, would be

$$\tilde{q} = \tilde{q}_m + pa, \quad a = \mathrm{e}\{-\mathrm{i}\theta/4 + \mathrm{i}m\pi/2\}. \tag{D 44}$$

Based on this, the asymptotic contribution from integrating across saddle point m in the a-direction would be

$$I_m = \frac{a\,\mathrm{e}^{r^{3/2}\phi(\tilde{q}_m)}}{\sqrt{2\pi|\phi''(\tilde{q}_m)|}\,r^{(2n+1)/4}}\,\frac{1}{\tilde{q}_m^n}(1 + O(r^{-3/2})), \tag{D 45}$$

https://doi.org/10.1017/jfm.2011.116 Published online by Cambridge University Press

$$I_0 = \frac{\exp\{-\frac{2}{3}r^{3/2}\,\mathrm{e}^{3\mathrm{i}\theta/2}\}}{2\sqrt{\pi}r^{1/4}\,\mathrm{e}^{\mathrm{i}\theta/4}} \times \begin{cases} 1 & n=0 \\ \dfrac{-\mathrm{i}}{\sqrt{r}}\,\mathrm{e}^{-\mathrm{i}\theta/2} & n=1 \\ \dfrac{-1}{r}\,\mathrm{e}^{\mathrm{i}\theta} & n=2 \end{cases}, \tag{D 46}$$

$$I_1 = \frac{\mathrm{i}\exp\{\frac{2}{3}r^{3/2}\,\mathrm{e}^{3\mathrm{i}\theta/2}\}}{2\sqrt{\pi}r^{1/4}\,\mathrm{e}^{\mathrm{i}\theta/4}} \times \begin{cases} 1 & n=0 \\ \dfrac{\mathrm{i}}{\sqrt{r}}\,\mathrm{e}^{-\mathrm{i}\theta/2} & n=1 \\ \dfrac{-1}{r}\,\mathrm{e}^{\mathrm{i}\theta} & n=2 \end{cases}. \tag{D 47}$$

We now consider which saddle points the steepest descent contour passes over. Figure 13 shows $\phi(\tilde{q})$ in the $\tilde{q}$-plane, together with the contour $\mathscr{C}$. This shows that, for $-2\pi/3 < \theta < 2\pi/3$, only the $m=0$ saddle point contributes, giving

$$f_0(r\,\mathrm{e}^{\mathrm{i}\theta}) \sim \frac{1}{2\sqrt{\pi}r^{1/4}\,\mathrm{e}^{\mathrm{i}\theta/4}} \exp\left\{-\frac{2}{3}r^{3/2}\,\mathrm{e}^{3\mathrm{i}\theta/2}\right\}, \tag{D 48a}$$

$$f_1(r\,\mathrm{e}^{\mathrm{i}\theta}) \sim \frac{-\mathrm{i}}{2\sqrt{\pi}r^{3/4}\,\mathrm{e}^{3\mathrm{i}\theta/4}} \exp\left\{-\frac{2}{3}r^{3/2}\,\mathrm{e}^{3\mathrm{i}\theta/2}\right\}, \tag{D 48b}$$

$$f_2(r\,\mathrm{e}^{\mathrm{i}\theta}) \sim \frac{-1}{2\sqrt{\pi}r^{5/4}\,\mathrm{e}^{5\mathrm{i}\theta/4}} \exp\left\{-\frac{2}{3}r^{3/2}\,\mathrm{e}^{3\mathrm{i}\theta/2}\right\}. \tag{D 48c}$$

For $2\pi/3 < \theta < 4\pi/3$, both saddle points and the pole at $\tilde{q}=0$ contribute, giving

$$f_0(r\,\mathrm{e}^{\mathrm{i}\theta}) \sim \frac{1}{2\sqrt{\pi}r^{1/4}\,\mathrm{e}^{\mathrm{i}\theta/4}} \left[\exp\left\{-\frac{2}{3}r^{3/2}\,\mathrm{e}^{3\mathrm{i}\theta/2}\right\} + \mathrm{i}\exp\left\{\frac{2}{3}r^{3/2}\,\mathrm{e}^{3\mathrm{i}\theta/2}\right\}\right], \tag{D 49a}$$

$$f_1(r\,\mathrm{e}^{\mathrm{i}\theta}) \sim \frac{-\mathrm{i}}{2\sqrt{\pi}r^{3/4}\,\mathrm{e}^{3\mathrm{i}\theta/4}} \left[\exp\left\{-\frac{2}{3}r^{3/2}\,\mathrm{e}^{3\mathrm{i}\theta/2}\right\} - \mathrm{i}\exp\left\{\frac{2}{3}r^{3/2}\,\mathrm{e}^{3\mathrm{i}\theta/2}\right\}\right] - \mathrm{i}, \tag{D 49b}$$

$$f_2(r\,\mathrm{e}^{\mathrm{i}\theta}) \sim \frac{-1}{2\sqrt{\pi}r^{5/4}\,\mathrm{e}^{5\mathrm{i}\theta/4}} \left[\exp\left\{-\frac{2}{3}r^{3/2}\,\mathrm{e}^{3\mathrm{i}\theta/2}\right\} + \mathrm{i}\exp\left\{\frac{2}{3}r^{3/2}\,\mathrm{e}^{3\mathrm{i}\theta/2}\right\}\right] + r\,\mathrm{e}^{\mathrm{i}\theta}, \tag{D 49c}$$

with the final term being the contribution from the pole.

REFERENCES

Abrahams, I. D. & Wickham, G. R. 2001 On transient oscillations of plates in moving fluids. *Wave Motion* **33**, 7–23.

Abramowitz, M. & Stegun, I. A. 1964 *Handbook of Mathematical Functions*, 9th edn. Dover.

Anderson, E., Bai, Z., Bischof, C., Blackford, S., Demmel, J., Dongarra, J., Du Croz, J., Greenbaum, A., Hammarling, S., McKenney, A. & Sorensen, D. 1999 *LAPACK Users' Guide*. Society for Industrial and Applied Mathematics.

Aurégan, Y., Starobinski, R. & Pagneux, V. 2001 Influence of grazing flow and dissipation effects on the acoustic boundary conditions at a lined wall. *J. Acoust. Soc. Am.* **109**, 59–64.

Brambley, E. J. 2009 Fundamental problems with the model of uniform flow over acoustic linings. *J. Sound Vib.* **322**, 1026–1037.

Brambley, E. J. 2011 A well-posed boundary condition for acoustic liners in straight ducts with flow. *AIAA J.* doi:10.2514/1.J050723.

https://doi.org/10.1017/jfm.2011.116 Published online by Cambridge University Press

Brambley, E. J. & Peake, N. 2006 Classification of aeroacoustically relevant surface modes in cylindrical lined ducts. *Wave Motion* **43**, 301–310.

Brambley, E. J. & Peake, N. 2008 Stability and acoustic scattering in a cylindrical thin shell containing compressible mean flow. *J. Fluid Mech.* **602**, 403–426.

Brazier-Smith, P. R. & Scott, J. F. 1984 Stability of fluid flow in the presence of a compliant surface. *Wave Motion* **6**, 547–560.

Campos, L. M. B. C. & Serrão, P. G. T. A. 1998 On the acoustics of an exponential boundary layer. *Phil. Trans. R. Soc. Lond.* A **356**, 2335–2378.

Crighton, D. G. & Oswell, J. E. 1991 Fluid loading with mean flow. I. Response of an elastic plate to localized excitation. *Phil. Trans. R. Soc. Lond.* A **335**, 557–592.

Eversman, W. 1971 Effect of boundary layer on the transmission and attenuation of sound in an acoustically treated circular duct. *AIAA J.* **49** (5), 1372–1380.

Eversman, W. & Beckemeyer, R. J. 1972 Transmission of sound in ducts with thin shear layers – convergence to the uniform flow case. *J. Acoust. Soc. Am.* **52**, 216–220.

Goldstein, M. & Rice, E. 1973 Effect of shear on duct wall impedance. *J. Sound Vib.* **30**, 79–84.

Hinch, E. J. 1991 *Perurbation Methods*. Cambridge.

Jones, D. S. 1977 The scattering of sound by a simple shear layer. *Phil. Trans. R. Soc. Lond.* A **284**, 287–328.

Koch, W. & Möhring, W. 1983 Eigensolutions for liners in uniform mean flow ducts. *AIAA J.* **21** (2), 200–213.

Landau, L. D. & Lifshitz, E. M. 1987 *Fluid Mechanics*, 2nd edn. Elsevier.

Lucey, A. D., Sen, P. K. & Carpenter, P. W. 2003 Excitation and evolution of waves on an inhomogeneous flexible wall in a mean flow. *J. Fluids Struct.* **18**, 251–267.

Mariano, S. 1971 Effect of wall shear layers on the sound attenuation in acoustically lined rectangular ducts. *J. Sound Vib.* **19**, 261–275.

Mungur, P. & Plumblee, H. E. 1969 Propagation and attenuation of sound in a soft-walled annular duct containing a sheared flow. *NASA* SP-207, 305–327.

Myers, M. K. 1980 On the acoustic boundary condition in the presence of flow. *J. Sound Vib.* **71**, 429–434.

Nagel, R. T. & Brand, R. S. 1982 Boundary layer effects on sound in a circular duct. *J. Sound Vib.* **85**, 19–29.

Nayfeh, A. H. 1973 Effect of the acoustic boundary layer on the wave propagation in ducts. *J. Acoust. Soc. Am.* **54**, 1737–1742.

Peake, N. 1997 On the behaviour of a fluid-loaded cylindrical shell with mean flow. *J. Fluid Mech.* **338**, 387–410.

Prangsma, G. J., Alberga, A. H. & Beenakker, J. J. M. 1973 Ultrasonic determination of the volume viscosity of N_2, CO, CH_4 and CD_4 between 77 and 300 K. *Physica* **64**, 278–288.

Pridmore-Brown, D. C. 1958 Sound propagation in a fluid flowing through an attenuating duct. *J. Fluid Mech.* **4**, 393–406.

Renou, Y. & Aurégan, Y. 2010 On a modified Myers boundary condition to match lined wall impedance deduced from several experimental methods in presence of a grazing flow. *AIAA Paper* 2010-3945.

Rice, E. J. 1969 Propagation of waves in an acoustically lined duct with a mean flow. *NASA Tech. Rep.* SP-207.

Richter, C. & Thiele, F. H. 2007 The stability of time explicit impedance models. *AIAA Paper* 2007-3538.

Rienstra, S. W. 2003 A classification of duct modes based on surface waves. *Wave Motion* **37**, 119–135.

Rienstra, S. W. 2007 Acoustic scattering at a hard–soft lining transition in a flow duct. *J. Engng Maths* **59**, 451–475.

Rienstra, S. W. & Peake, N. 2005 Modal scattering at an impedance transition in a lined flow duct. *AIAA Paper* 2005-2852.

Riley, K. F., Hobson, M. P. & Bence, S. J. 2002 *Mathematical Methods for Physics and Engineering*, 2nd edn. Cambridge.

https://doi.org/10.1017/jfm.2011.116 Published online by Cambridge University Press

Schlichting, H. 1968 *Boundary-Layer Theory*, 3rd edn. McGraw-Hill.

Tam, C. K. W. & Auriault, L. 1996 Time-domain impedance boundary conditions for computational aeroacoustics. *AIAA J.* **34** (5), 917–923.

Tester, B. J. 1973 Some aspects of 'sound' attenuation in lined ducts containing inviscid mean flows with boundary layers. *J. Sound Vib.* **28**, 217–245.

Vilenski, G. G. & Rienstra, S. W. 2007 On hydrodynamic and acoustic modes in a ducted shear flow with wall lining. *J. Fluid Mech.* **583**, 45–70.

https://doi.org/10.1017/jfm.2011.116 Published online by Cambridge University Press